

UNCLASSIFIED

AD NUMBER

ADB014104

LIMITATION CHANGES

TO:

Approved for public release; distribution is unlimited.

FROM:

Distribution authorized to U.S. Gov't. agencies only; Test and Evaluation; NOV 1975. Other requests shall be referred to Air Force Materials Laboratory, Nonmetallic Materials Division, Elastomers and Coatings Branch, AFML/MBE, Wright-Patterson AFB, OH 45433.

AUTHORITY

afwal ltr, 19 nov 1982

THIS PAGE IS UNCLASSIFIED

THIS REPORT HAS BEEN DELIMITED
AND CLEARED FOR PUBLIC RELEASE
UNDER DOD DIRECTIVE 5200.20 AND
NO RESTRICTIONS ARE IMPOSED UPON
ITS USE AND DISCLOSURE.

DISTRIBUTION STATEMENT A

APPROVED FOR PUBLIC RELEASE,
DISTRIBUTION UNLIMITED.

AFML-TR-76-5

AD B014104

INVESTIGATION OF CONTAMINATION EFFECTS ON THERMAL CONTROL MATERIALS

MCDONNELL DOUGLAS ASTRONAUTICS COMPANY • EAST
SAINT LOUIS, MISSOURI 63166
MCDONNELL DOUGLAS CORPORATION

MARCH 1976

TECHNICAL REPORT AFML-TR-76-5

FINAL TECHNICAL REPORT 15 MAY 1974 - 14 AUGUST 1975



Distribution limited to U.S. Government agencies only; (test and evaluation) November 1975. Other requests for this document must be referred to the Air Force Materials Laboratory, Nonmetallic Materials Division, Elastomers and Coatings Branch, AFML/MBE, Wright-Patterson Air Force Base, Ohio 45433.

AD No. _____

DDC FILE COPY

AIR FORCE MATERIALS LABORATORY
AIR FORCE WRIGHT AERONAUTICAL LABORATORIES
AIR FORCE SYSTEMS COMMAND
WRIGHT-PATTERSON AIR FORCE BASE, OHIO 45433

NOTICE

When Government drawings, specifications, or other data are used for any purpose other than in connection with a definitely related Government procurement operation, the United States Government thereby incurs no responsibility nor any obligation whatsoever; and the fact that the government may have formulated, furnished, or in any way supplied the said drawings specifications, or other data, is not to be regarded by implication or otherwise as in any manner licensing the holder or any other person or corporation, or conveying any rights or permission to manufacture, use, or sell any patented invention that may in any way be related thereto.

This technical report has been reviewed and is approved for publication.

Brian C. Price
BRIAN C. PRICE, 1st Lt. USAF
Project Monitor

For the Commander:

Merrill L. Minges
MERRILL L. MINGES, Chief
Elastomers and Coatings Branch
Non-Metallic Materials Division

ACQUISITION FOR	
NTIS	White Section <input checked="" type="checkbox"/>
DDC	Red Section <input type="checkbox"/>
UNANNOUNCED	
JUSTIFICATION	
BY _____	
DISTRIBUTION/AVAILABILITY CODES	
Dist.	_____
B	

Copies of this report should not be returned unless return is required by security considerations, contractual obligations, or notice on a specific document.

UNCLASSIFIED

SECURITY CLASSIFICATION OF THIS PAGE (When Date Entered)

REPORT DOCUMENTATION PAGE		READ INSTRUCTIONS BEFORE COMPLETING FORM	
1. REPORT NUMBER AFML-TR-76-5	2. GOVT ACCESSION NO.	3. RECIPIENT'S CATALOG NUMBER	
4. TITLE (and Subtitle) INVESTIGATION OF CONTAMINATION EFFECTS ON THERMAL CONTROL MATERIALS.		5. TYPE OF REPORT & PERIOD COVERED Final Technical Report. 15 May 1974 - 14 Aug 1975	
7. AUTHOR(s) T. A. Hughes T. E. Bonham T. H. Allen		6. CONTRACT OR GRANT NUMBER(s) F33615-73-C-5091	
9. PERFORMING ORGANIZATION NAME AND ADDRESS McDonnell Douglas Astronautics Company - EAST McDonnell Douglas Corporation, P.O. Box 516, St. Louis, Mo. 63166		10. PROGRAM ELEMENT, PROJECT, TASK AREA & WORK UNIT NUMBERS Project 7340 Task 07	
11. CONTROLLING OFFICE NAME AND ADDRESS Air Force Materials Laboratory (AFML/MBE) Air Force Systems Command Wright-Patterson Air Force Base, Ohio 45433		12. REPORT DATE March 1976	
14. MONITORING AGENCY NAME & ADDRESS (if different from Controlling Office) Thomas A. Hughes, Thomas E. Bonham, Thomas H. Allen, Rodney M. F. Linford		13. NUMBER OF PAGES 75	
		15. SECURITY CLASS. (of this report) UNCLASSIFIED	
		15a. DECLASSIFICATION/DOWNGRADING SCHEDULE	
16. DISTRIBUTION STATEMENT (of this Report) Distribution limited to U.S. Government Agencies only; (test and evaluation); November 1975. Other requests for this document must be referred to the Air Force Materials Laboratory Nonmetallic Materials Division, Elastomers and Coatings Branch, AFML/MBE, Wright-Patterson Air Force Base, Ohio 45433.			
17. DISTRIBUTION STATEMENT (of the abstract entered in Block 20, if different from Report) 1284p.			
18. SUPPLEMENTARY NOTES 16 AF-7340 12734007			
19. KEY WORDS (Continue on reverse side if necessary and identify by block number) Contamination Coatings, Colorants, and Finishes Optical Properties Optics Outgassing Laser Communications Spacecraft Scattering Polarization Mixing			
20. ABSTRACT (Continue on reverse side if necessary and identify by block number) Contamination kinetics studied on thick films from DC-704 and RTV-602 (commercial grade) using both infrared ellipsometry and quartz crystal microbalances, confirmed that monomers experience constant deposition rates and reevaporation rates, while polymers have an exponential decay in such areas. Kinetics data was also obtained on a purified form of RTV-602 which showed significantly lower outgassing rates, and on SR-585 silicone adhesive. Limited data was also obtained for RTV's -106 and -560. Measurements were made to obtain effective			

DD FORM 1 JAN 73 1473

EDITION OF 1 NOV 65 IS OBSOLETE

UNCLASSIFIED

SECURITY CLASSIFICATION OF THIS PAGE (When Date Entered)

403 930 AB

UNCLASSIFIED

SECURITY CLASSIFICATION OF THIS PAGE (When Data Entered)

molecular weight data on outgassing species and their vapor pressure. However, the molecular weight data was not considered reliable due to its wide scatter. The effects of specific contaminants, such as multilayer insulations, a non-reflective black paint, and a bonded silica fabric, was determined on critical properties of different substrates. Contaminants from one multilayer insulation and the black paint were found to produce extensive scattering effects on a plane mirror, and significant changes in solar absorptance of a second surface mirror when the contamination was in excess of about 500 Å thick.

Studies made of the outgassing rates of two candidate systems being considered for silica fabric thermal control system indicated that the purified version of RTV-602 was superior to SR-585. Potential materials that might be used as Reststrahlen reflectors to reduce the effects of an electromagnetic encounter were identified. Also the effect of contamination on a dielectric stack proposed for this same purpose was examined. The effect of contamination at 3.8 μm wavelength was much more pronounced than its effect on 10.6 μm properties. The effect of contamination on polarization mixing of the laser communication system optics was experimentally measured and compared with calculated values.

UNCLASSIFIED

SECURITY CLASSIFICATION OF THIS PAGE (When Data Entered)

PREFACE

This report describes the results of work conducted under Contract F33615-73-C-5091-P00002 by the McDonnell Douglas Astronautics Company-East, St. Louis, Missouri. The work is a part of Project 7340-07, "Coatings For Energy Utilization, Control, and Protective Functions", and was administered by the Elastomers And Coatings Branch of The Air Force Materials Laboratory, Air Force Systems Command, Wright-Patterson Air Force Base, Ohio. Project Engineer for AFML/MBE was Lt. Brian Price. Program Manager for MDAC-E was Mr. Thomas A. Hughes. Principal MDC contributors to the program were Mr. Thomas E. Bonham, Mr. Thomas H. Allen, and Dr. Rodney M. F. Linford.

This report covers the period of 15 May 1974 to 14 August 1975, and was submitted 14 November 1975. Work conducted during the prior period of 14 May 1973 to 14 May 1974 has been reported in Technical Report AFML-TR-74-218.

Boo 42834

TABLE OF CONTENTS

	<u>PAGE</u>
I INTRODUCTION	1
II SUMMARY AND CONCLUSIONS	2
III TASK 1 - STUDY OF BASIC CONTAMINATION KINETICS	5
A. Thick Film Kinetics.	6
1. Test Technique	7
2. Results	9
a. DC-704 Diffusion Pump Oil	9
b. RTV-602 (Commercial Grade)	12
c. Modified RTV-602	15
B. Vapor Pressure and Molecular Weight Determinations	17
1. Equipment and Procedure	20
2. Test Results	23
a. DC-704 Silicone Oil	23
b. RTV-602	27
3. Discussion of Results	29
IV TASK 2 - EVALUATION OF SPECIFIC CONTAMINANT-SUBSTRATE COMBINATIONS	31
A. Solar Absorption of Contaminated Irradiated Thermal Control Surfaces	32
1. Materials Evaluated	32
2. Test Results	33
B. Scattering Measurements On Contaminated Solar Reflectors	38
1. Measurement Technique	39
2. Scattering Results	43

TABLE OF CONTENTS (Cont'd)

	<u>PAGE</u>
a. Insulation No. 1	43
b. Insulation No. 2	43
c. Westinghouse Black Paint	47
C. Total Weight Loss and Collected Volatile Condensable	
Material Tests	47
V TASK 3 - KINETICS OF LOW OUTGASSING MATERIALS	
A. AFML/HAC RTV-602	52
B. SR-585	54
C. Relative Accumulation of Contaminants	54
VI TASK 4 - SELECTIVE REFLECTORS	57
A. Reststrahlen Reflectors	57
B. Contamination of Dielectric Stacks	61
VII TASK 5 - CONTAMINATION OF LASER SYSTEM OPTICS	65
A. Experimental Technique	66
B. Results	67
VIII REFERENCES	74

LIST OF ILLUSTRATIONS

	<u>PAGE</u>
1 Optical Arrangement Of Ellipsometer And Sample Chamber	8
2 Test Arrangement For Simultaneous Ellipsometer And QCM Measurements	8
3 Deposition And Reevaporation Of Contaminant From DC-704 On Gold Mirror	10
4 Deposition And Reevaporation Of Contaminant From DC-704 QCM Data	11
5 Deposition And Reevaporation Of RTV-602	13
6 Reevaporation Rate Of Contaminant From RTV-602	14
7 Deposition And Reevaporation Of RTV-602	16
8 Thickness History Of Deposition And Reevaporation of AFML/HAC RTV-602 On Gold Mirror	18
9 Experimental Arrangement For Measuring Vapor Pressure And Mole- cular Weight	22
10 Typical Sequence Of Vapor Pressure Measurements	23
11 Vapor Pressure Of DC-704	25
12 Reevaporation Rate Of DC-704	26
13 Vapor Pressure Of RTV-602	28
14 Solar Absorptance of SR-585 Contaminated And Irradiated Second Surface Mirror	35
15 Laser-Goniometer System For Scattering Measurement	40
16 Laser-Goniometer Scattering Measurement	41
17 Contaminant From Insulation No. 1 On Silver Mirror	44
18 Scattering Due To Contamination From Insulation No. 1	45
19 Contaminant From Insulation No. 2	46
20 Scattering Due to Contamination From Insulation No. 2	48

LIST OF ILLUSTRATIONS (Continued)

	<u>PAGE</u>
21 Contaminant From Westinghouse Black Paint	49
22 Scattering Due To Contamination From Westinghouse Black Paint .	50
23 Deposition Rates And Reevaporation Rates of AFML/HAC RTV-602 .	53
24 Deposition Rates and Reevaporation Rates of SR-585.	55
25 Relation Between Absorption Index And Index of Refraction To Obtain Various Levels of Reflectivity	59
26 Reststrahlen Peaks	60
27 Reflectance Of A 21-Layer Dielectric Stack At 10.6 μ m Wavelength With A Silicone Contaminant On The Surface	63
28 Reflectance Of A 21-Layer Dielectric Stack At 3.8 μ m Wavelength With A Silicone Contaminant On The Surface	64
29 Polarization Mixing As A Function Of Contaminant Thickness - RTV-106/Gold Mirror	68
30 Polarization Mixing As A Function Of Contaminant Thickness - RTV-560/Gold Mirror	69
31 Calculated Polarization Mixing Due To An Organic Film On A Gold Mirror ($n = 1.50$, $k = 0$)	71
32 Polarization Mixing As A Function of Contaminant Thickness. Three Layer Dielectric Stack On A Gold Mirror. Contaminant RTV 106	72
33 Polarization Mixing As A Function Of Contaminant Thickness. Five-Layer Dielectric Stack On A Gold Mirror. Contaminant From RTV-106	73

I. INTRODUCTION

The effects of contamination on a spacecraft or satellite and upon the specific mission has frequently been of an insidious nature. The presence of contamination frequently can only be inferred by instrument aberrations, or by special detectors installed for that purpose, unless the vehicle is returned to earth and physically examined. The effects of the contamination on the spacecraft can take a variety of forms. It can critically degrade the α_s/ϵ ratio of the thermal control surfaces and result in spacecraft temperatures higher than allowable for mission objectives; it can seriously impair the performance of optical elements to the extent that they provide inadequate signals or resolution, or even spurious data. Contamination can also affect vulnerability to an EM encounter.

McDonnell Douglas Astronautics Company at St. Louis initiated work under Air Force Contract F33615-73-C-5091 in May 1973 to study contamination kinetics and effects. Results of the first year of the program have been reported previously in AFML-TR-74-218. The work conducted under the second year of the program is described in the present report.

The current work has consisted of the five tasks given below and are reported in the sequence listed.

- o Study of Basic Contamination Kinetics
- o Evaluation of Specific Contaminant-Substrate Combinations
- o Kinetics of Low Outgassing Materials
- o Selective Reflectors
- o Contamination of Laser System Optics

II. SUMMARY AND CONCLUSIONS

During this term of the program, contamination kinetics were studied for RTV-602 (commercial and purified grades), and SR-585, and limited kinetics data was obtained on RTV's -106 and -560. Measurements were also made to obtain molecular weight of outgassing species and their vapor pressure for use on contamination modeling. However, the molecular weight data was not considered reliable due to its inconsistency.

The effects of specific contaminants on critical optical properties of specific substrates were measured. This included as source contaminants two multilayer insulations, a nonreflective black paint, and a new concept in thermal control materials, silica fabric bonded to a spacecraft surface. The measurements included changes in solar absorptance, scattering effects, and total weight loss and vacuum condensable materials. Studies were also made of the outgassing rates of two candidate adhesive systems being considered for the silica fabric thermal control system.

A review was made for potential materials that might be used as Reststrahlen reflectors to reduce the effects of an electromagnetic encounter. Also, the effect of contamination on a dielectric stack proposed for this same purpose was examined.

The effect of contamination on polarization mixing of the laser communications system optics was experimentally measured and compared with calculated values.

Among the pertinent observations made during this program were:

- o Verification has been obtained that the kinetics of monomeric and polymeric contaminants follow differing laws. Previous results were limited to films thinner than about 400\AA , and have now been extended to about four times that thickness. Measurements were confirmed with dual results from QCM data and infrared ellipsometry. Monomers are shown to evaporate at a constant rate, while polymers evaporate with an exponential decay rate. The longer wavelength infrared ellipsometry eliminated the previous problem of spurious results due to nonhomogenous film scattering at shorter (visible) wavelengths.

- o The purified version of RTV-602, developed by Hughes Aircraft Co., was found to be a significant improvement over the standard RTV-602 in terms of outgassing, though it is not the equal of RTV-566 in that respect.
- o Determination of molecular weights of outgassing species by simultaneous measurement of deposition rates and vapor pressure was not successful. The inconsistencies in the data argue in favor of finding alternate procedures for this determination.
- o A second surface mirror contaminated with outgassed products from SR-585 silicone adhesive displayed significant changes in solar absorptance when the contaminant thickness was in excess of about 500Å. Subsequent irradiation produced further small changes that were difficult to assess as the changes were comparable to the accuracy of the measurement.
- o Contaminant from one multilayer insulation and from a nonreflecting black paint introduced substantial scattering on a plane mirror. Contaminant from another multilayer insulation introduced much less scattering. A major difference between the two insulations was that the high scatter sample contained a glass scrim reinforcement, though it is not certain that the debris on the mirror originated with the glass fibers. Also, this insulation would not be acceptable under the tentative NASA standards for the micro-VCM test as it had a weight loss in excess of 1%. The insulation which produced low scattering results was within the NASA standards for total weight loss and volatile condensable material.
- o The effect of contamination on a dielectric stack on an optical element acts to introduce an additional layer to the stack. On the particular stack design studied, calculations indicated that contamination introduces only small changes in reflectance at 10.6 μm wavelength, but results in large variations in reflectance at 3.8 μm wavelength. Similar net changes in transmission can be expected at those wavelengths.

- o Contamination was found to introduce large changes in the polarization mixing of plane mirrors, and was also found to be different from that calculated from theoretical considerations. The difference was believed due to the fact that a contaminant film frequently departs from an idealized homogenous, optically isotropic film. Significant polarization mixing can result in a serious degradation of signal levels in a laser communications system data transmissions to earth receivers.

III. TASK 1 - STUDY OF BASIC CONTAMINATION KINETICS

The purpose of this study was to determine in greater detail the kinetics which control outgassing rates and reevaporation rates of contaminants. The study concentrated on two areas: thick film measurements, and basic properties of the source species (vapor pressure and molecular weights).

Experimental data for monomeric contaminants have indicated that the reevaporation rate γ , Å/min, is constant for films thicker than a few monolayers, up to at least 200Å. However, reevaporation data for contaminant films deposited from RTV-602 (polymeric compound) and other similar sources exhibited linear characteristics over only a limited thickness range, and subsequent limited experiments on thicker films, using both a quartz crystal microbalance (QCM) and ellipsometric methods, revealed distinctly nonlinear kinetics for films up to 450Å thick (Reference 1). The results of these experiments also showed that scattering of visible radiation by small agglomerates of the contaminant complicated the interpretation of ellipsometer data taken at a wavelength of 0.6328 μm when the films were greater than 250Å thick.

It was desired to measure the deposition and reevaporation characteristics of typical polymeric contaminants up to a much greater thickness range (1000-1500Å thick), and to verify the differences noted between monomeric and polymeric films. It was further desired to make these measurements by two independent means using both ellipsometry and a QCM. To avoid the limitations placed on ellipsometry (by apparent scattering) when using a visible wavelength laser (0.6328 μm), the ellipsometer was modified to use a 3.39 μm wavelength laser source and which greatly increased its immunity to film structuring.

Current computer modeling approaches to contamination are usually based on concepts employing the Langmuir equation for predicting outgassing rates:

$$w = \frac{P}{17.14} \sqrt{\frac{M}{T}} \quad (1)$$

where

- w = mass loss per unit area and time, g/cm² sec
- P = vapor pressure, torr
- M = molecular weight of outgassed species
- T = absolute temperature, K

Two requirements immediately arise in using the Langmuir equation. First, the vapor pressure must be known at the existing temperature, or known as a function of temperature by the Claussius-Clapeyron relationship. Secondly, the molecular weight of the evaporating species must be known, and which may be different than the base material. Because our data indicated that either, or both, the vapor pressure and molecular weight of contaminants from polymeric materials was changing with time, attempts were made to measure both of these during the course of outgassing. This was done by simultaneously measuring the pressure within the VES while monitoring deposition rates with the ellipsometer. To gain confidence in this technique, initial tests were made with a stable monomer of known molecular weight, and later with a polymeric silicone. However, these tests were not successful in providing reproducible molecular weight data.

A. Thick Film Kinetics

Deposition and reevaporation rates were measured for DC-704 diffusion pump oil, RTV-602 silicone compound (commercial grade), and a low outgassing grade of RTV-602 developed by Hughes Aircraft Co. (Reference 2). The DC-704 was included to verify the previously noted differences in behavior of contaminants from monomeric materials compared to polymeric materials. The tests were also conducted using both the infrared ellipsometer technique and a quartz crystal microbalance (QCM).

The concept that the deposition and reevaporation of polymeric films have an exponential relationship with time (as well demonstrated here) is not totally incompatible with earlier data by others which showed a constant rate. The basic exponential relationship is:

$$\overset{\circ}{A} = \overset{\circ}{A}_0 e^{-mt} \quad (2)$$

where $\overset{\circ}{A}$ is the thickness at time t , and $\overset{\circ}{A}_0$ is the initial amount at time zero. Therefore, the fraction of the original material remaining at time t is:

$$\frac{\overset{\circ}{A}}{\overset{\circ}{A}_0} = e^{-mt} \quad (3)$$

and expanding the right hand side in series form,

$$\frac{\overset{\circ}{A}}{A} = 1 + (-mt) + \frac{(-mt)^2}{2!} + \frac{(-mt)^3}{3!} + \dots$$

and as a first approximation, retaining only the first two terms on the right:

$$\frac{\overset{\circ}{A}}{A_0} = 1 - mt$$

If $\frac{\overset{\circ}{A}}{A_0}$ is the fraction remaining, then the fraction lost, W , is $1 - \frac{\overset{\circ}{A}}{A_0}$, and.

$$W = 1 - [1 - mt]$$

$$W = mt$$

(4)

Thus, as a first approximation, the thickness (or mass) lost is a linear function of time. However, at long time periods, it becomes increasingly inaccurate to drop terms in the series expansion. Data contained in this report follows the more exact exponential form.

1. Test Technique

All measurements were made in a vacuum chamber equipped with an ellipsometer as described in Reference 1. The contaminant was contained in a vapor effusion source (VES) (a modified Knudsen cell) with the multiorifice nozzle (10 orifices, each 0.020 in. dia in a ring configuration). The test arrangement is shown in Figures 1 and 2.

The IR ellipsometer was obtained by modifying the visible ellipsometer already installed on the vacuum ellipsometer chamber. The visible polarizing optics were replaced by calcite IR transmitting optics, and the silicon photodetector used in the visible regime was replaced by a lead sulfide IR detector. The IR light source was a Spectra Physics model 125 HeNe laser. This laser is over one meter long, and because of its length it had to be installed in an adjoining room. The beam was directed to the ellipsometer by reflecting optics with the beam path enclosed by hollow plastic tubing to protect the beam from scattering due to dust particles and to provide safety to personnel. This laser was used because it has interchangeable end mirrors which allows selection of either the .633 μ m visible line or the 3.39 μ m line.

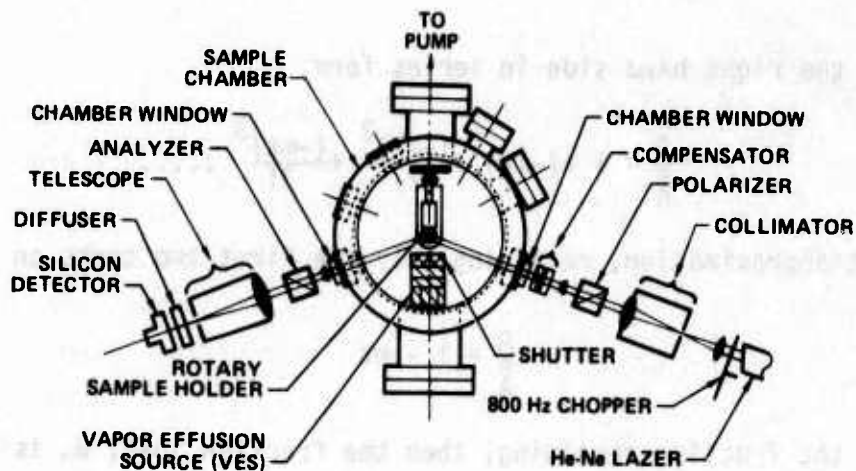


Figure 1 Optical Arrangement of Ellipsometer and Sample Chamber

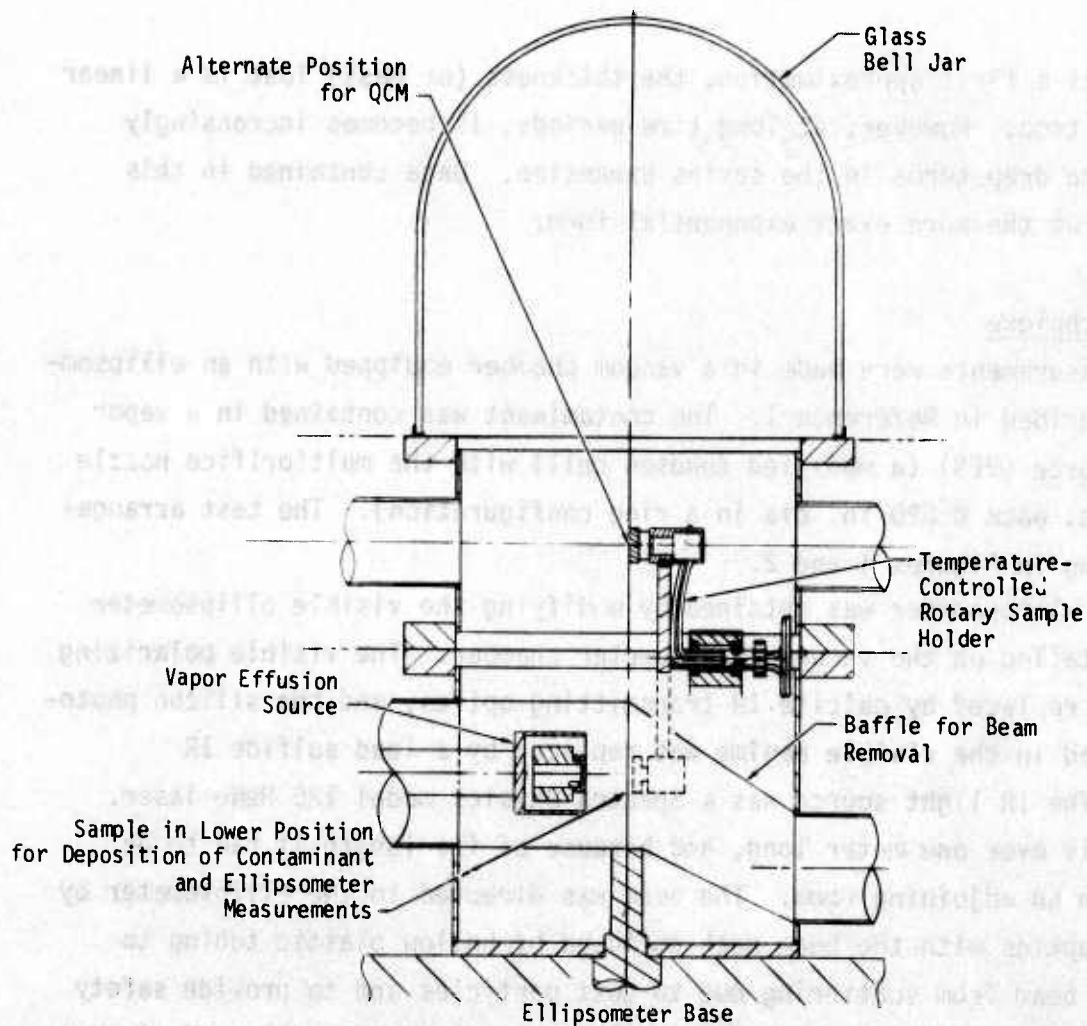


Figure 2 Test Arrangement for Simultaneous Ellipsometer and QCM Measurements

This capability was especially useful when alignment was necessary. The .633 μm mirrors were installed to provide a visible beam for alignment purposes, and then they were switched to the 3.39 μm mirrors for IR operation. In practice, there was some slight adjustment required to peak-out the beam alignment after changing the mirrors, but overall the alignment was accomplished with ease.

Inside the chamber, the QCM and the gold coated mirror were mounted at opposite ends of a rotatable bracket. One position of the bracket centered the gold sample in the molecular beam path from the shuttered Knudsen Cell and in the ellipsometer beam. The QCM was in the upper portion of the chamber for this case. The opposite bracket position interchanged the QCM and gold sample locations. The sample was exposed alternately to the contaminant source in the Knudsen cell with the QCM by opening the Knudsen cell shutter for an appropriate length of time while the particular surface was in the correct position. The reevaporation of the films was measured with the gold sample in the lower position for ellipsometric measurement. No matter what its position, the QCM was continuously monitored by means of a frequency counter and printer. All measurements were made in-situ within the vacuum chamber which was typically at about 10^{-6} torr pressure.

2. Results

(a) DC-704 Diffusion Pump Oil - Initial test runs were made with DC-704 silicone diffusion pump oil and the deposition and reevaporation are shown in Figure 3 (ellipsometer data) and Figure 4 (QCM data). The vapor effusion source (VES) was operated at 118.5°C for this deposition, and the substrates were at 25°C . The QCM data in Figure 4 was corrected from mass per unit area data (which the QCM measures) to thickness in angstroms by using the known specific gravity of DC-704. Both sets of data show generally constant deposition and reevaporation rates as expected (except the QCM data below $\sim 50\text{\AA}$ thickness, which was also expected). The measured deposition rates in the separate tests were: ellipsometer, $97.6 \text{ \AA}/\text{min}$; and QCM, $104.7 \text{ \AA}/\text{min}$ (VES temperature 118.5°C). The reevaporation rate of DC-704 in the ellipsometer test was $3.18 \text{ \AA}/\text{min}$, and in the QCM run, $5.22 \text{ \AA}/\text{min}$. The latter data represents the straight line portion of the curve prior to the thin film effects.

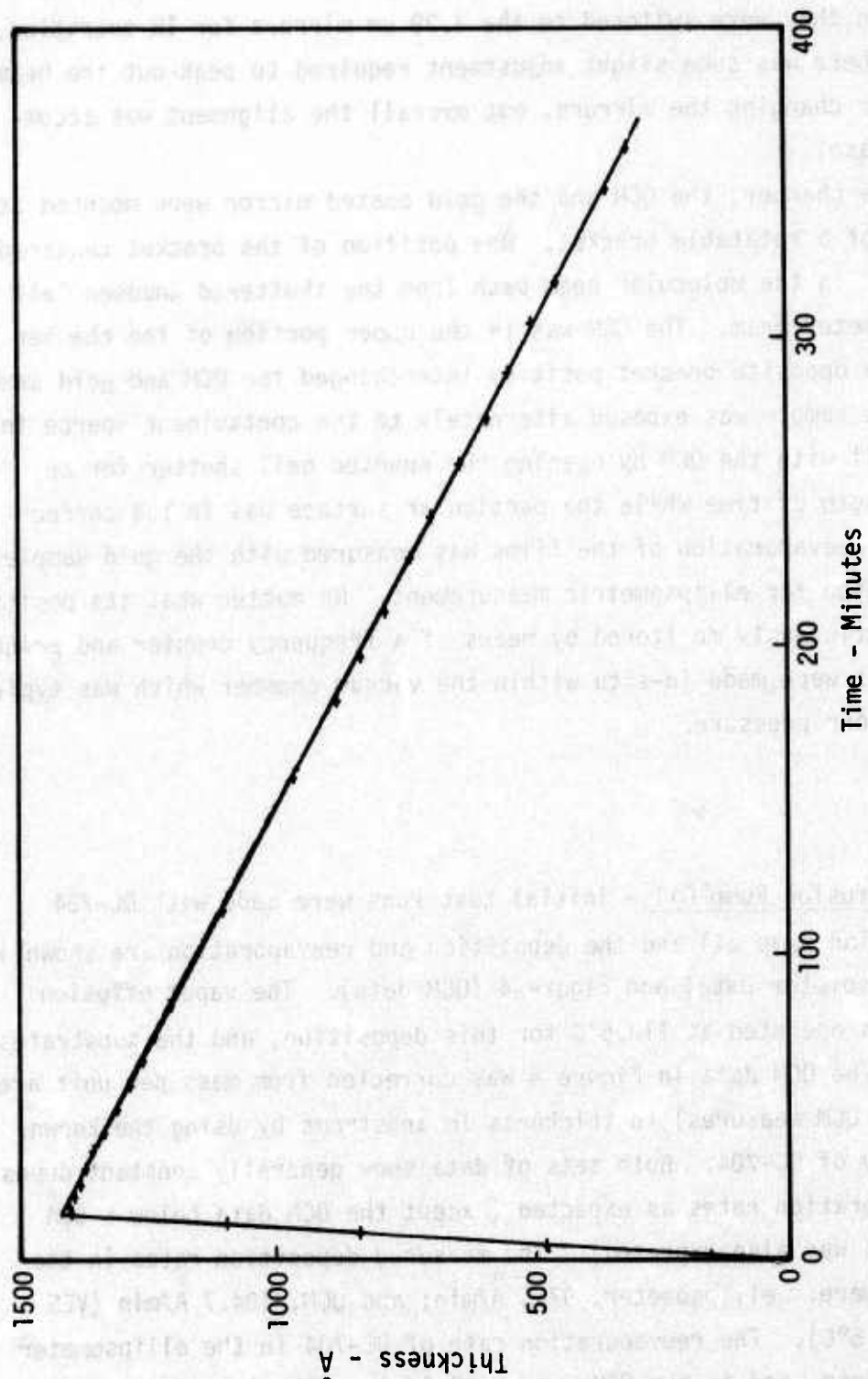


Figure 3 Deposition and Reevaporation of Contaminant from DC-704 on Gold Mirror - Ellipsometer Data

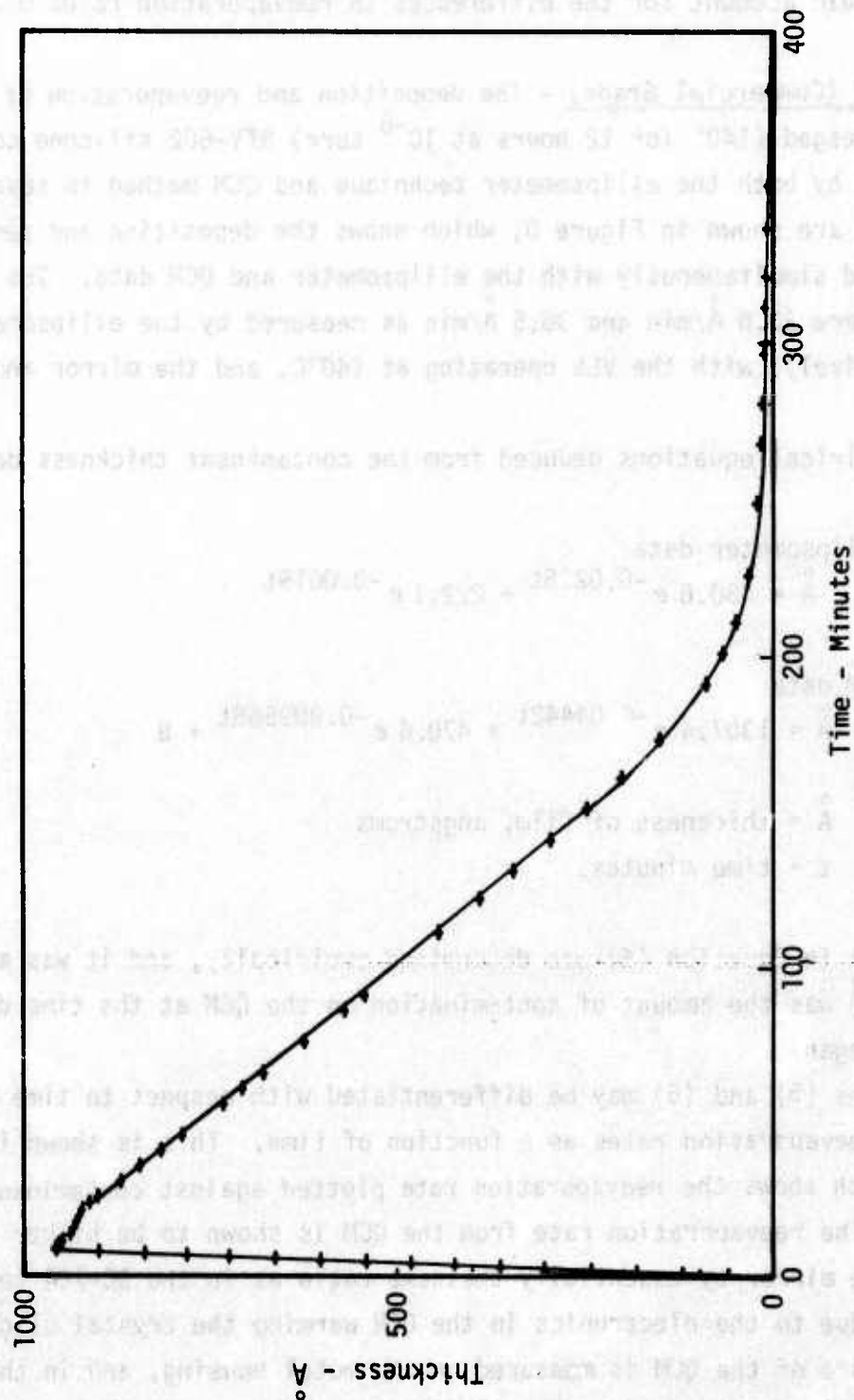


Figure 4 Deposition and Reevaporation of Contaminant from DC-704 QCM Data

The differences between the two reevaporation rates are most likely due to minor differences in temperature. At 25°C, a difference in temperature of about 3°C would account for the differences in reevaporation rates measured.

(b) RTV-602 (Commercial Grade) - The deposition and reevaporation of cured and preaged (140° for 12 hours at 10⁻⁶ torr) RTV-602 silicone compound was measured by both the ellipsometer technique and QCM method in several runs. Typical data are shown in Figure 5, which shows the deposition and reevaporation measured simultaneously with the ellipsometer and QCM data. The deposition rates were 33.6 Å/min and 36.5 Å/min as measured by the ellipsometer and QCM, respectively, with the VES operating at 140°C, and the mirror and QCM at 25°C.

The empirical equations deduced from the contaminant thickness data were:

ellipsometer data

$$\bar{A} = 430.6 e^{-0.0225t} + 222.1 e^{-0.0019t} \quad (5)$$

QCM data

$$\bar{A} = 1307.4 e^{-0.04442t} + 470.4 e^{-0.009568t} + 8 \quad (6)$$

where

\bar{A} = thickness of film, angstroms
t = time minutes.

The last term in Equation (6) was determined empirically, and it was also noted that 8Å was the amount of contamination on the QCM at the time deposition on the QCM began.

Equations (5) and (6) may be differentiated with respect to time to obtain the reevaporation rates as a function of time. This is shown in Figure 6 which shows the reevaporation rate plotted against contaminant film thickness. The reevaporation rate from the QCM is shown to be higher than that from the mirror by essentially the same ratio as in the DC-704 tests. This may be due to the electronics in the QCM warming the crystal slightly. The temperature of the QCM is measured on the metal housing, and in the vacuum chamber there could be a slight disparity in temperature.

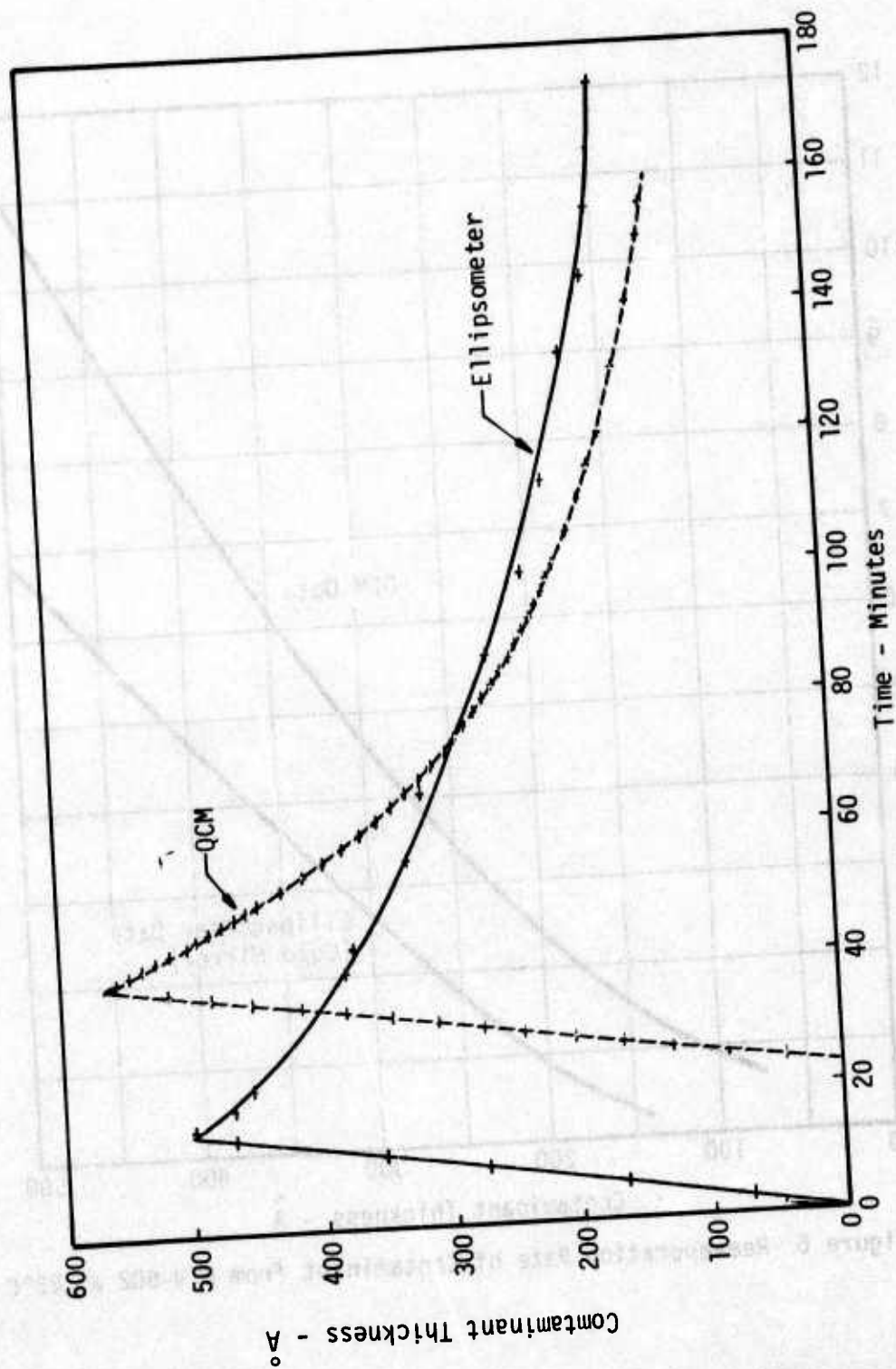


Figure 5 Deposition and Reevaporation of RTV-602

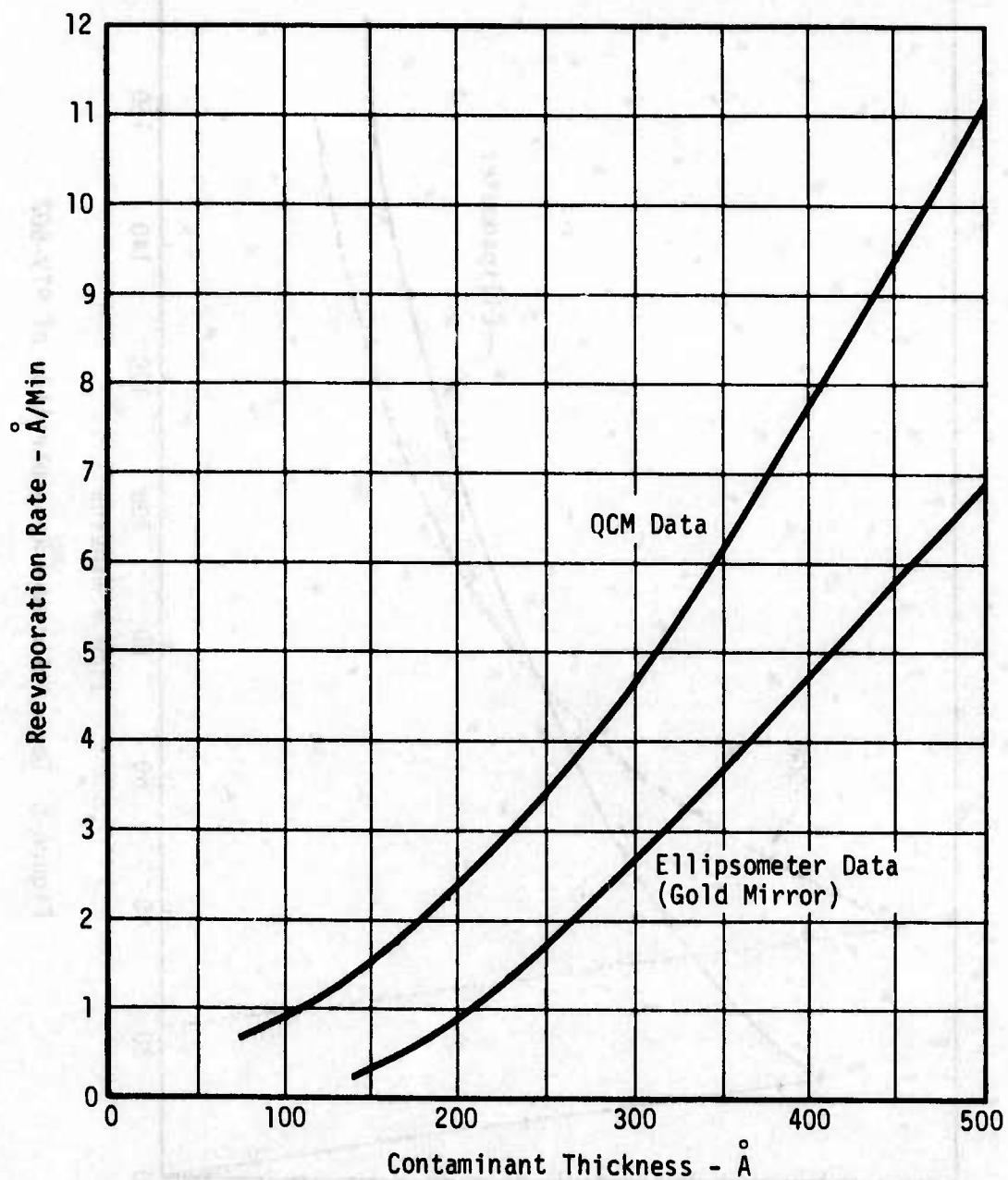


Figure 6 Reevaporation Rate of Contaminant from RTV-602 at 25°C

Another test run was made using the same sample of RTV-602, but this time depositing 1020 Å of contaminant on the QCM. Test data for this test are shown in Figure 7. This figure shows the initial cross-contamination of the QCM prior to the deposition, and the thickness buildup after the shutter was opened. The deposition was temporarily broken off for two brief periods for ellipsometer measurements, and immediately resumed. A decay in the deposition rate was noted (it also occurred in the previous run), presumably due to aging in the VES at 140°C during the long deposition period. The measured rates over the following time periods were noted:

50-69 minutes	24.1 Å/min
72-94 minutes	20.3 Å/min
96-103 minutes	16.3 Å/min

The reevaporation of the contaminant from the QCM is best correlated with the following empirical equation:

$$\overset{\circ}{A} = 3.529 \times 10^{15} e^{-0.3031t} + 2292.7 e^{-0.01433t} + 552 e^{-0.001074t} \quad (7)$$

where the time, t , is measured from the start of the test -- the same time base shown on Figure 7. With the thicker level of contamination, a three component reevaporation is noted, in comparison with the two component system detected earlier with thinner buildups.

The reevaporation rates of this test, as a function of thickness, were significantly lower than the previous test. This is believed due to the further aging of the source material in the VES, and which was also reflected in the lower deposition rates.

(c) Modified RTV-602 - Hughes Aircraft Company, under contract to AFML (Reference 2) has developed a low outgassing version of RTV-602, and which was evaluated for outgassing and reevaporation in this program. The standard TWL and CVCML was also determined and is reported in Section IV of this report. The purified base stock and catalyst used in this program was provided by AFML.

Test specimens were prepared by mixing and curing at room temperature the purified RTV-602 with 0.2% of tetramethylguanidine (in a 5% hexane solution).

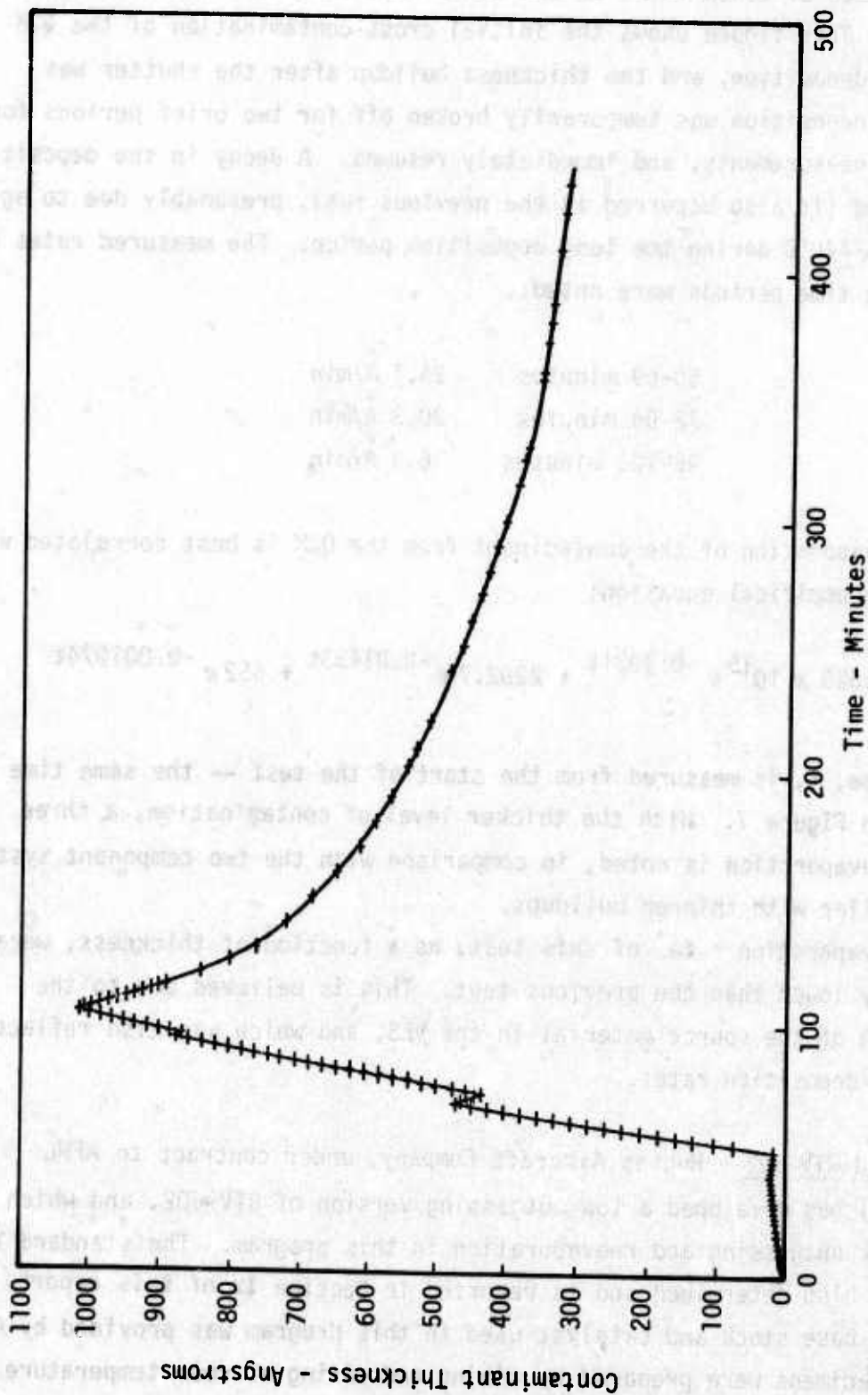


Figure 7 Deposition and Reevaporation of RTV-602 QCM at 25°C

Our usual procedure was followed in casting a film about 1/16 in. thick, and after curing, dicing into 1/16 in. cubes for loading into the VES.

The deposition rate and reevaporation rate of the AFML/HAC modified RTV-602 was initially measured using the VES with the standard 10 orifice annular ring nozzle. At 140°C VES temperature, no significant deposit was obtained on either the gold mirror or the QCM receivers, indicating an extremely low contamination potential for the material. Further tests were then made in an effort to get numerical data, using a single nozzle orifice on the VES which had 5 times the total orifice area of the previously used ring nozzle. The ellipsometer data (gold mirror) is shown in Figure 8. The initial buildup of contaminant was made using the VES at 140°C. Because the obviously low rate would not allow a buildup to the desired thickness within a reasonable time, the shutter was closed while the VES was heated to 180°C. The deposition at that temperature (beginning at 60 min in Figure 8) was allowed to continue until contaminant slightly in excess of 800Å was accumulated, when the film was allowed to reevaporate (beginning at 168 minutes). The reevaporation rate at 25°C, also shown on Figure 8, was very low, as would be expected for a low volatility material. The final data point, shown at the edge of the figure, was at 1284 minutes when the thickness was 416Å.

The measured deposition rate of the AFML/HAC modified RTV-602 was 3.14 Å/min at 140°C and the initial rate at 180°C was 13.2 Å/min. Because the VES orifice area was 5 times that used for the commercial RTV-602, caution must be exercised in making direct comparisons of the data on the two materials. The reevaporation data shows a definite trend to a multiple component system and a reasonably good fit is obtained with the empirical relationship:

$$\overset{\circ}{A} = 735.5 e^{-0.000444t} + 10629 e^{-0.025t} \quad (8)$$

where t is the time base shown on Figure 8. The time base if desired can be easily translated to time "0" at the beginning of reevaporation by appropriate changes to the constants.

B. Vapor Pressure and Molecular Weight Determinations

Determination of molecular weights employed a reversal of the classical Knudsen technique, which is used to estimate vapor pressure from weight loss

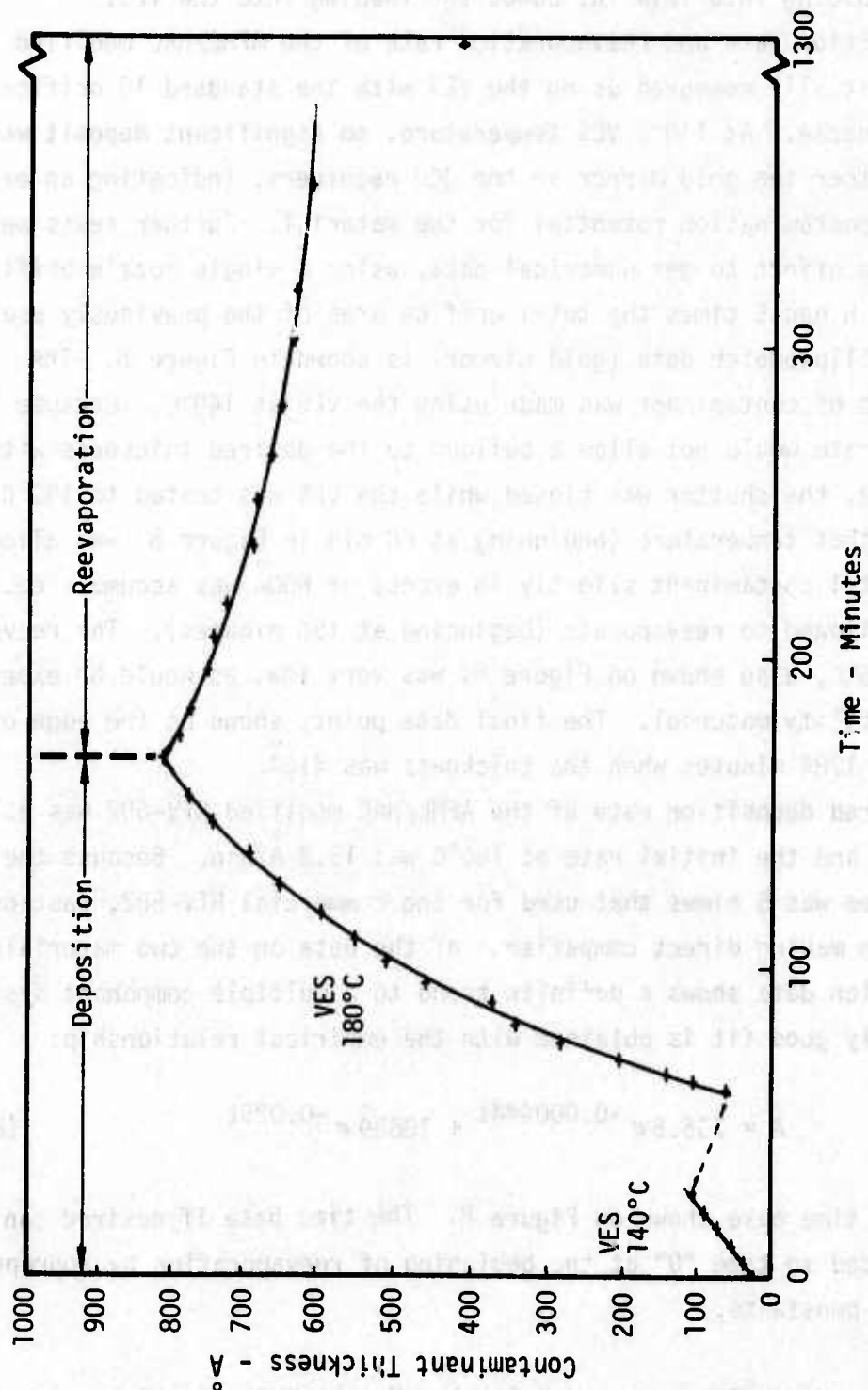


Figure 8 Thickness History of Deposition and Reevaporation of AFML/HAC RTV-602 on Gold Mirror

data of materials of known molecular weights. Our procedure was to measure the vapor pressure within the Knudsen cell (VES) in addition to the deposition rate, and then solve for the unknown molecular weight. The basic Knudsen equation is:

$$w = \frac{Pa}{17.14 \pi s} \sqrt{\frac{M}{T}} \quad (9)$$

and from which:

$$M = \left[\frac{17.14 \pi s^2}{a} \right]^2 \left(\frac{w}{P} \right)^2 T \quad (10)$$

where

M = molecular weight

w = deposition rate, g/cm² sec

P = vapor pressure, torr

T = temperature, K

a = orifice area, cm²

s = distance of substrate from orifice.

The basic Knudsen equation is valid when the angle over which material is collected (measured normal to the plane of the orifice plate) is small, the thickness of the orifice plate is small compared to the orifice diameter, and the orifice diameter is less than about 10% of the mean free path of the escaping gases. Correction factors are available if any of these limitations are exceeded.

Measurement of the evaporation rate, w, was by the usual ellipsometric technique on a sample placed in the molecular beam from the VES. The rate of thickness increase of the contaminant deposited on the cooled mirror was measured and converted to mass rate using the known specific gravity of the deposit. This technique assumes that the molecular beam is uniform at the plane of the mirror within the area of measurement, a condition that has been verified previously.

1. Equipment and Procedure

A prime requirement for the measurement of the vapor pressure within the Knudsen cell (VES) was that it be totally independent of the molecular weight of the gases present. This ruled out the use of the more common vacuum measuring techniques, such as ionization gauges. It was for this reason that a capacitance manometer gauge was used for the vapor pressure measurements. It is one of the few methods available which can measure pressures as low as 10^{-5} torr, independently of gas constitution.

The essential operating principal of the capacitance manometer employs a metal membrane stretched between fixed electrodes situated closely on each side. The membrane is vacuum sealed along its edges, thus creating two separate chambers. One chamber is connected to a source of known gas pressure for reference, and the other chamber is connected to the source of unknown gas pressure. A difference in pressure between the chambers causes a deflection of the dividing membrane which in turn causes a corresponding change in the capacitance between the membrane and each electrode. This change in capacitance is read by an AC bridge circuit which is calibrated to the pressure difference. True gas pressure (force per unit area) is determined this way, giving a reading that is independent of gas or vapor composition. Thus, this method is ideally suited in principle to the objectives of measuring molecular weight.

The apparatus used in these experiments was a Baratron gauge manufactured by MKS Instruments, Inc., Burlington, Massachusetts. The system consisted of a model 94AH-1 head with separate bakeable sensor, model 170M-6A electronics unit, and a model 170M-25B digital readout. The features of this system include a head bakeable to 450°C and operable to 150°C , pressure range 10^{-5} to 1 torr, and stated accuracy of 0.1% to 0.25% of reading. Front panel controls on the electronics unit permit initializing the readout to zero.

Initially, the Baratron sensor head was installed in the ellipsometer vacuum chamber with the unknown pressure side connected to the Knudsen cell by means of a short length of tubing. The reference side was left open to the vacuum system ambient pressure which was measured simultaneously by a vacuum ionization gauge and readout. With this setup, the Baratron was reading the gas pressure within the Knudsen cell at all times. Typical chamber pressures recorded by the chamber ionization gauge at the beginning of a test were

1×10^{-6} torr. With the Knudsen cell heated the chamber pressure generally rose to about 3×10^{-6} torr. Whether this change reflected a true change in pressure, or was the result of changing gas composition (air to air plus contaminant) is uncertain. However, this chamber pressure was about two decades lower than the lowest pressure recorded for the Knudsen cell by the Baratron. Therefore, the Baratron pressure difference was accepted as the absolute pressure within the Knudsen cell. Throughout these measurements, the Baratron sensor head and connecting tubing were heated to 140°C to prevent vapor condensation within the pressure sensing system.

The first tests with this setup were conducted to determine the correctness of the method. DC-704 vacuum pump oil was used as the contaminant because it has been well-characterized in past experiments and is known to have no aging phenomenon associated with it. In addition it has a known molecular weight and vapor pressure. A typical sequence of procedures for these tests was to begin with a new charge of material in the cell, pump down the system, zero the Baratron readout, then begin heating the cell. However, the Baratron readout would begin to indicate pressure almost immediately, at temperatures well below the point where the DC-704 should have had a measurable vapor pressure. This occurrence appeared to be caused by zero instability of the pressure gauge. Attempts to eliminate or reduce this effect were not successful, consequently the apparatus was modified to the form shown in Figure 9.

The tubing between the Knudsen cell and the Baratron sensor was lengthened to permit the installation of a two-way valve between the sensor and cell. One position of the valve connected the unknown side of the sensor to the cell the same way as before, while the other position connected the unknown side to the vacuum system ambient pressure. For the latter valve position, both chambers of the sensor would experience the same pressure (ambient vacuum chamber pressure), thus permitting the readout to be adjusted to zero whenever desired. In this way the effects of zero instability were expected to be eliminated. It was necessary to locate the valve close to a vacuum flange so that an externally controlled actuator could be installed. This required a tubing length of approximately 35 cm which was less than an ideal arrangement, but was unavoidable.

The operating procedure employed in these tests was to keep the Baratron sensor head divorced from the VES while the latter was heated to its operating

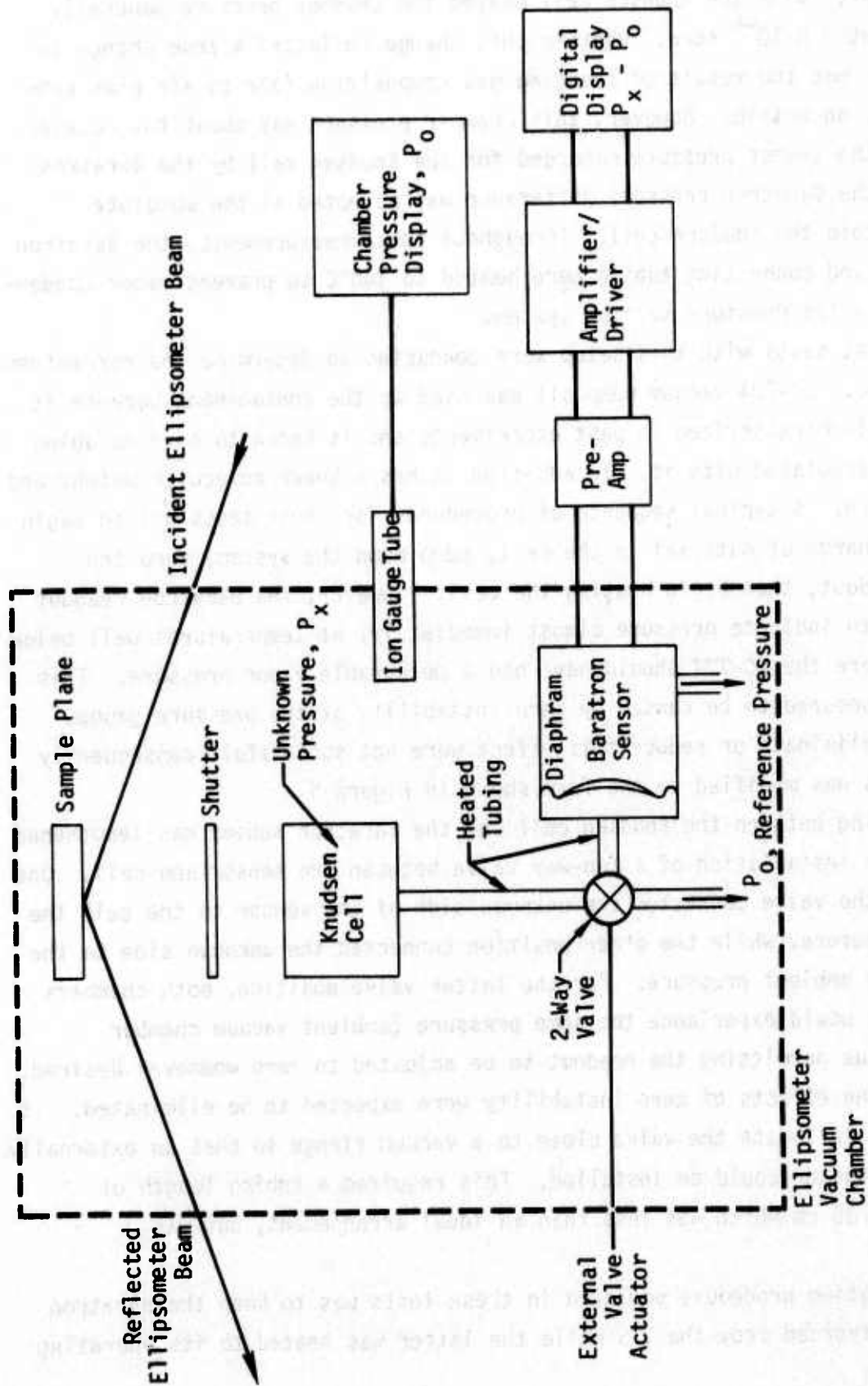


Figure 9 Experimental Arrangement for Measuring Vapor Pressure and Molecular Weight

temperature. The sensor head and tubulature were also heated simultaneously. The indicated pressure difference displayed on the Baratron readout during this period was a negative pressure -- even though both sides of the Baratron were exposed to the chamber vacuum. When the temperature of the VES and sensor head were stabilized at the operating temperature and the Baratron indicated a stable pressure, the Baratron readout was rezeroed, the valve position switched to the VES and the vapor pressure measured when the readout reached a stabilized value. The valve position was then recycled back to the open (chamber) position and a new indicated "zero" pressure noted. For reasons unknown, the second "zero" was usually higher than the initial zero pressure reading. The sequence of the indicated pressure readings is shown in Figure 10. The variations in the "zero" pressures made the interpretation of the data difficult at times due to the uncertainty of which was the true zero. It was also noted that any change in heater voltage also caused the pressure indication to change. This was somewhat strange as the signal from the sensor head to the indicator was a frequency signal, not a voltage signal.

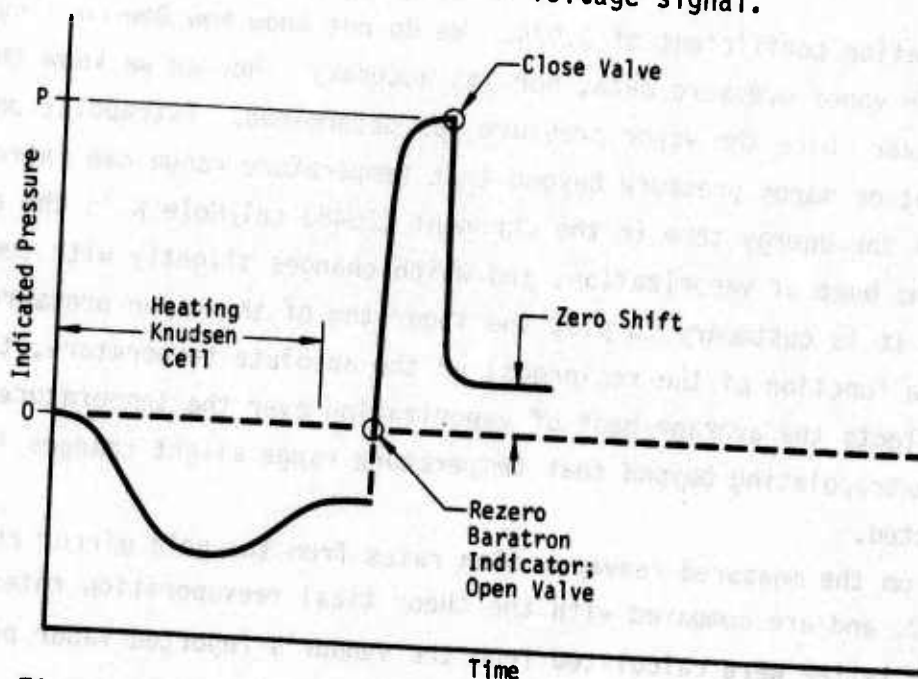


Figure 10 Typical Sequence of Vapor Pressure Measurements

2. Test Results

(a) DC-704 Silicone Oil - Initial tests were made with DC-704 silicone oil to obtain experience with a material of known molecular weight, and equally

important, of unchanging molecular weight due to aging, and to establish confidence in the technique. The vendor (Dow-Corning) reported data on DC-704 is:

Composition - tetramethyltetraphenyltrisiloxane

Molecular weight - 484

$$\text{Vapor pressure } P = 1.059 \times 10^{11} e^{-\frac{25483}{RT}} \quad (11)$$

where

P = vapor pressure, torr

R = gas constant, 1.987 cal/mole K

T = temperature, K

Figure 11 shows the vapor pressure data as a function of temperature, and compared to the vendor's equation. The best fit of the experimental data is represented by

$$P = 5.03 \times 10^{17} e^{-\frac{37670}{RT}} \quad (12)$$

with a correlation coefficient of 0.974. We do not know how Dow-Corning obtained their vapor pressure data, nor its accuracy. Nor do we know the temperature over which the vapor pressure was determined. Extrapolation of an Arrhenius plot of vapor pressure beyond that temperature range can introduce some error as the energy term in the exponent (25483 cal/Mole K in the case of DC-704) is the heat of vaporization, and which changes slightly with temperature. While it is customary to plot the logarithm of the vapor pressure as a straight line function of the reciprocal of the absolute temperature, the slope obtained reflects the average heat of vaporization over the temperature range. Thus, when extrapolating beyond that temperature range slight changes in slope may be expected.

Data from the measured reevaporation rates from the gold mirror are shown in Figure 12, and are compared with the theoretical reevaporation rates of DC-704. The latter were calculated from the vendor's reported vapor pressure and molecular weight by the Langmuir equation.

Prior to the reevaporation rate measurements noted above, measured deposition data for DC-704 indicated sticking coefficients ranging from 0.85 at 26.4°C to 0.39 at 32.5°C. Considerable thought has been given as to whether such coefficients should also be applied to the reevaporation rates. Our tentative conclusion is that they do not apply during reevaporation, and

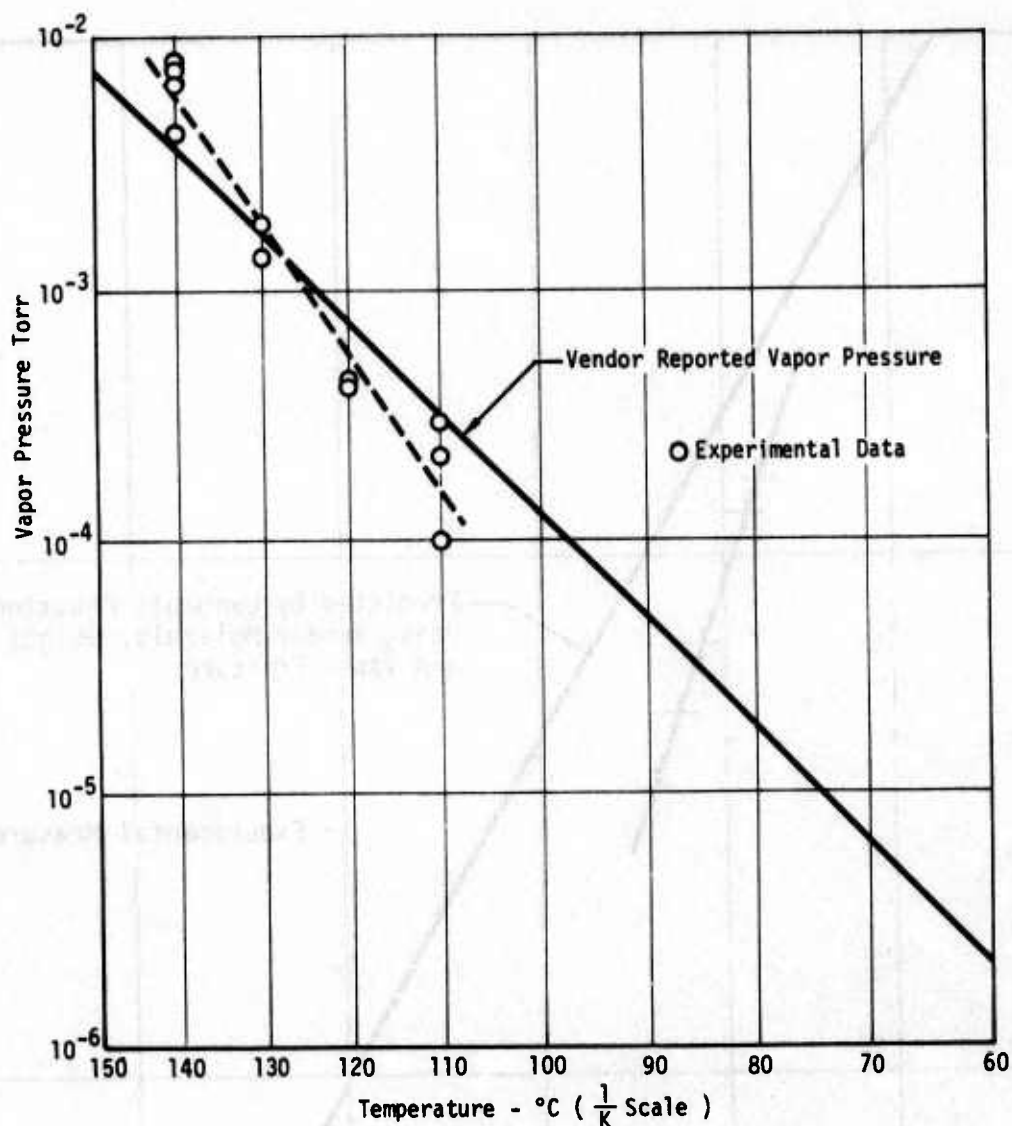


Figure 11 Vapor Pressure of DC-704

the data shown in Figure 12 do not include any correction for evaporation coefficients.

In the development of the Langmuir equation for evaporation and the Knudsen equations for Knudsen cells, constants called condensation coefficients and evaporation coefficients (not to be confused with accommodation coefficients, which are associated with the exchange of energy between gas molecules and liquid or solid surfaces) are included. The condensation coefficient equals the fraction of molecules incident on the surface of the condensed phase, which condense. It is generally assumed that the condensation coefficient and coefficient of evaporation are equal, and also equal unity, except for cases where there may be foreign contamination, and are therefore usually

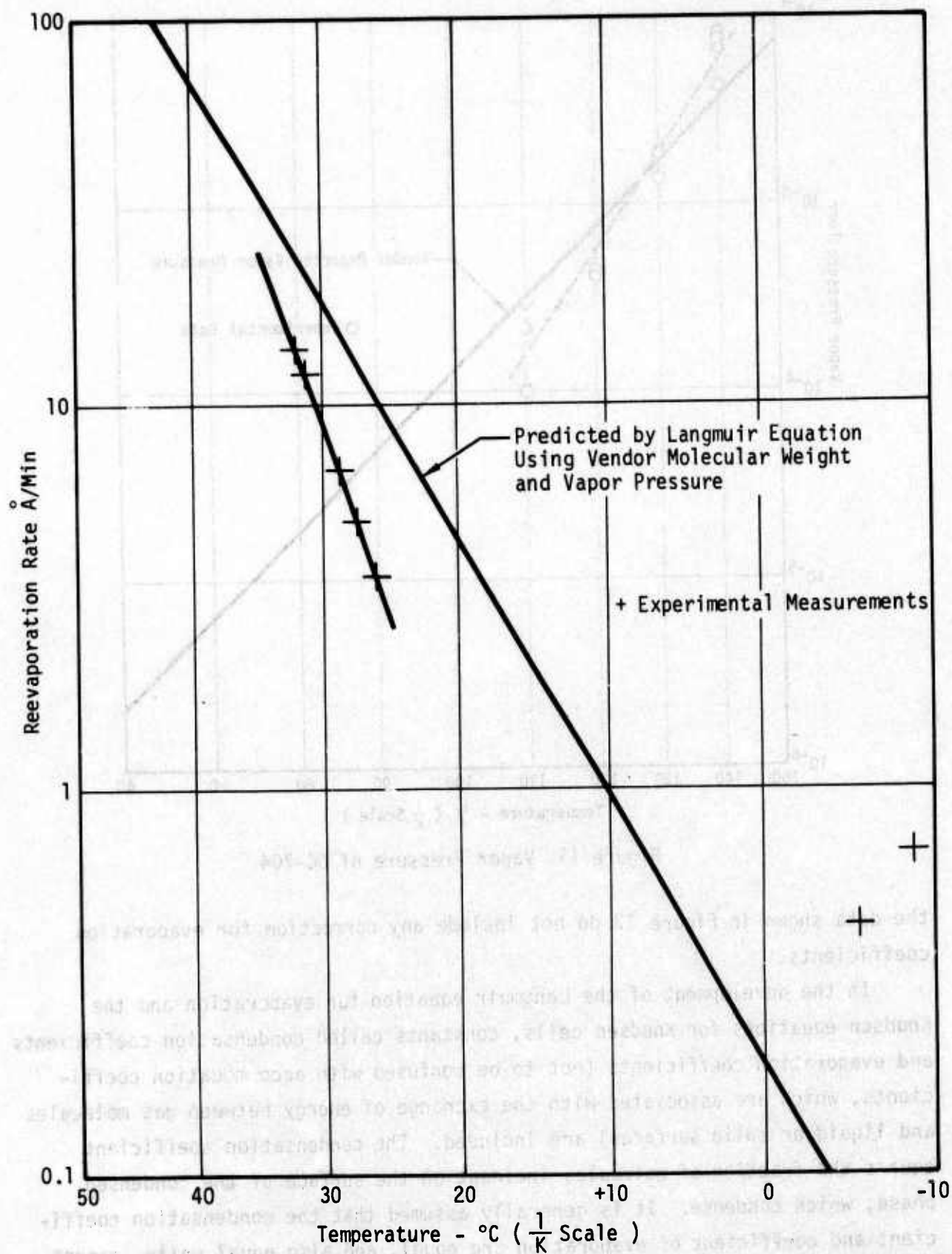


Figure 12 Reevaporation Rate of DC-704

omitted in the final equations. There is an inherent assumption in the development of the equations that the evaporating source and the molecules in the vapor state returning and condensing on the source are equal in temperature.

There appears to be a fine distinction between the condensation coefficients and what we measure and refer to as sticking coefficients. In the former, the vapor and condensed phase are at the same temperature, while in the latter case, the substrate is at a much lower temperature than the incident gas. And, during later reevaporation from the substrate, the temperature of the condensed phase and the evaporating specie become equal, resulting in an evaporation coefficient of unity. It is interesting to note that in any thorough discussion of the evaporation coefficient in the Langmuir equation, the authors are careful to note that it is not the accommodation coefficient; however, it is beginning to appear that the sticking coefficient may indeed be related to the accommodation coefficient when the source and condensation surfaces are at different temperatures.

The measured deposition rates on the chilled mirror and the measured vapor pressure at the time of deposition provided calculated molecular weights for DC-704 of 279, 247, 668, 759, and 1762, a totally unsatisfactory spread in the results. Examining the solution of the Langmuir equation for M , the molecular weight, it may be noted that both the outgassing rate and vapor pressure terms are squared, so that a very high degree of accuracy of both of these measurements is necessary.

To insure that the Knudsen cell pressure was essentially the true vapor pressure (the orifice in any Knudsen cell allows a slight deviation from equilibrium), a new orifice plate was made. This contained only a single orifice, 0.020 in. diameter in an 0.005 in. thick plate. Test results with this nozzle were only slightly better, yielding molecular weights of 192, 316, and 341.

(b) RTV-602 - Test runs were also made with the commercial grade of RTV-602 (not preconditioned) at VES temperatures of 140°C and 120°C. The values of the calculated molecular weights while ridiculously low (5.5 to 51), did show a progressive increase with age in the VES. The measured vapor pressure also decayed exponentially with age in the VES, as shown in Figure 13. This decay appears similar in nature to the decay in deposition rates we have

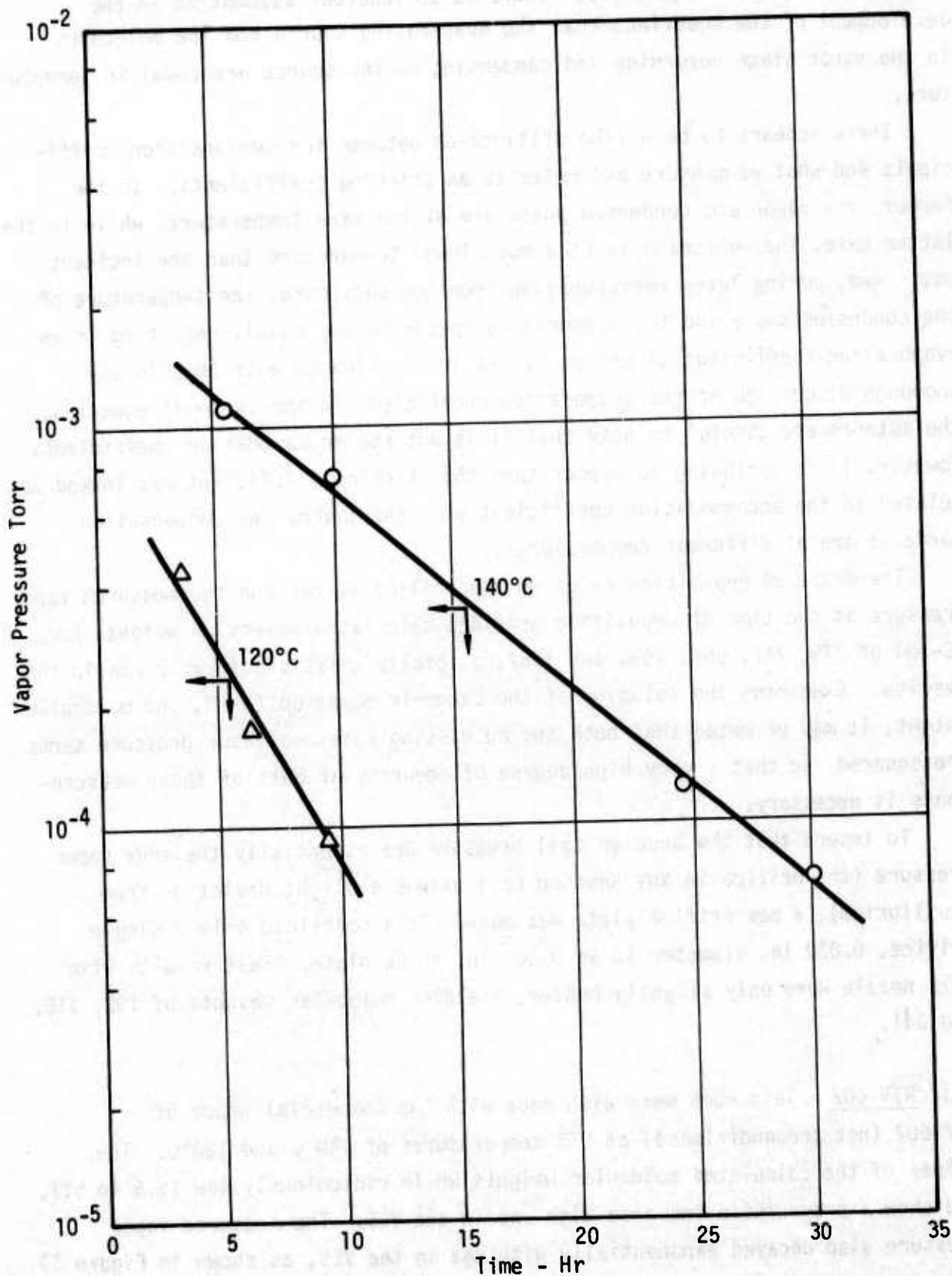


Figure 13 Measured Vapor Pressure of RTV-602

experienced with RTV-602. The empirical equations describing the vapor pressure are:

$$P_{140^{\circ}\text{C}} = 2.18 \times 10^{-3} e^{-0.115t} \quad (13)$$

$$P_{120^{\circ}\text{C}} = 9.82 \times 10^{-4} e^{-0.251t} \quad (14)$$

where P is in torr, and t in hours. The correlation coefficients for these equations are 0.9988 and 0.994, respectively. The data for each of the temperatures were begun with fresh samples of unconditioned, cured RTV-602.

3. Discussion of Results

The attempt to obtain molecular weights of outgassing products by simultaneous measurements of vapor pressure and deposition rates was not successful. Test runs with monomeric material (DC-704 silicone oil) did not provide reproducible results; consequently, results obtained with a material of unknown molecular weight would be subject to serious question.

The tests with DC-704 were run many times and all presently known techniques to improve the results were applied without success. This included making a new orifice plate for the VES (Knudsen cell) with a much smaller orifice in a very thin wall. This was to insure that the measured pressure was indeed the equilibrium vapor pressure (too large an orifice area can result in lack of equality, an inherent assumption in Knudsen cell work). The thin wall also minimizes deviations from theoretical flow. These steps did not appreciably improve the results.

A probable cause of the lack of reproducibility of molecular weights is believed due to the extremely high degree of precision required in measuring the vapor pressure in the VES, and the deposition rates. In rearranging the Knudsen equation for determining molecular weight, the square of the ratio of deposition rate to vapor pressure occurs and thus the technique is extremely sensitive to the accuracy of both of these measurements.

Due to the time constraints of the program, it appeared prudent to transfer our efforts to the remaining tasks in order to accomplish the maximum results within the time and funds available.

It is recognized that some approaches to computer modeling require this type of data. Whether future efforts to measure vapor pressure/molecular weights will be more successful is uncertain at this time. Consequently, those modeling efforts incorporating this approach can be expected to be seriously hampered until this type of experimental procedure is successfully accomplished.

IV. TASK 2 - EVALUATIONS OF SPECIFIC CONTAMINANT - SUBSTRATE COMBINATIONS

This study was designed to measure changes in selected optical properties of specific combinations of source contaminants and sensitive substrates used in critical satellite applications. These tests included:

- o Changes in the solar absorptance of thermal control materials (metallized Teflon and a second surface mirror) when contaminated by outgassing products from multilayer thermal insulations, and from silicone adhesives.
- o The effect on the specular reflectance of a plane mirror when the mirror contaminated by material from the two multilayer insulations, and from a nonreflective black paint.
- o Determination of the total mass loss, and collected volatile condensable materials by standard techniques.

The specific tests made are outlined in the table below. Those tests in which negative results were obtained are noted. This usually occurred when the outgassing rates were so low that it was not possible to obtain a sufficient accumulation of contamination on the substrate to have a measurable effect.

<u>Contaminant</u>	<u>Substrate</u>	<u>Measurement</u>	<u>Radiation</u>	<u>Comments</u>
Insulation 2	Al/FEP	α_s	-	No results
HAC/RTV-602	Al/FEP	α_s	-	No results
SR-585/Fabric	SSM	α_s	UV, e^- , p^+	
Insulation 1	Ag mirror	scattering	none	
Insulation 2	Ag mirror	scattering	none	
Black Paint	Ag mirror	scattering	none	
Insulation 1	-	TWL, CVCM	-	
Insulation 2	-	TWL, CVCM	-	
SR-585/Fabric	-	TWL, CVCM	-	

A. Solar Absorptance of Contaminated Irradiated Thermal Control Surfaces

These tests employed the trilevel vacuum test chamber (Reference 1) as it has facilities for deposition from a VES in the lower level; UV, electron, and proton radiation sources at the middle level; and an in-situ integrating sphere with a Beckman DK-2A spectrophotometer for measuring solar absorptance at the upper level. The sample was rotated among the levels as desired by an externally controlled arm.

The test procedure was to load the contaminant into the VES, with the critical substrate directly opposite the nozzle of the VES. The contaminant flux issuing from the VES was measured by rotating the substrate out of the molecular beam at intervals and substituting a quartz crystal microbalance (QCM) in its place. To reflect operational conditions the substrates were cryogenically cooled. Because the cooling was a slow process due to the thermal contact resistance in the vacuum chamber, deposition was initiated once the substrate was cooled to -25°C . The cooling continued during deposition, the substrates usually reaching -120°C . The QCM was cooled by radiation exchange with a cryogenically cooled shroud, and the QCM was usually at -15°C or colder. Thus the sticking coefficients on the substrate and on the QCM crystal surface were both essentially 1.0. For these tests it was desired to obtain fairly thick films ($\sim 1000\text{\AA}$) of contaminant, as previous results (Reference 1) indicated that contaminant thicknesses of only several hundred angstroms had negligible effects on solar absorptance.

1. Materials Evaluated

The specific materials evaluated as sources of contamination were provided by the Air Force Materials Laboratory and were identified as multilayer insulations currently employed in spacecraft, and a silicone adhesive (SR-585) used to bond silica fabric (a passive thermal control material) to the surface of a spacecraft. The multilayer insulation specimens consisted of:

Insulation No. 1

Aluminized Kapton (1 mil) reinforced with glass scrim

10 layers of alternating 1/4 mil/aluminized Mylar and 1/8 in. honeycomb pattern Nylon net

Aluminized Kapton (1 mil) reinforced with glass scrim

Insulation No. 2

Aluminized Teflon (FEP) outer layer (2.5 mils thick)

Nylon net - 1/8 in. honeycomb pattern

10 layers of alternating aluminized Mylar (0.25 mil) and Nylon net

The Hughes Aircraft Co. modification of RTV-602 used here has been described in a previous section. This material has a potential use as an adhesive for the silica fabric thermal control material. The SR-585, a General Electric Co. silicone adhesive, was also being considered for the same application.

The substrates on which changes in solar absorptance were to be determined were aluminized Teflon (FEP) film and a second surface mirror. The latter was 10 mil thick fused silica with silver vapor deposited on one surface.

2. Test Results

The first combination tested was Insulation Blanket No. 2 (contaminant) with aluminized FEP Teflon as the substrate. Using a large orifice Knudsen cell (5 times the nozzle area of the multiorifice nozzle) operating at a temperature of 180°C and the substrate initially at -43°C, the initial deposition rate was 2.5Å/min which dropped to zero after two hours. The estimated total deposit was only 92Å at the end of the two hours. This thickness was considered insufficient to affect the solar reflectance, and the overall outgassing was obviously too small to present a contamination problem. This test was repeated with a fresh sample of insulation blanket and similar results were obtained: an estimated 70Å deposit over a 75 minute period when the deposition rate (as measured by the QCM) decayed to zero. No further testing with this material and substrate was attempted due to the negative results.

The operating temperature of 180°C was considered unrealistically high and could possibly cause decomposition of the material, leading to outgassing products unrepresentative of the original material. All further testing was limited to a maximum operating temperature of the Knudsen cell of 140°C.

The second combination tested was Astroquartz fabric bonded to aluminum foil with AFML/HAC RTV-602. This specimen was placed flat on the base of the Knudsen cell with the fabric face parallel to and facing the orifice. Aluminized FEP Teflon was the cooled substrate. Results with the cell at 140°C showed an initial deposition rate of 1.5Å/min (at 10 minutes) and zero after 60 minutes. The contaminant accumulation was too small to warrant reflectance measurements, and testing was ended at this point.

The combination of Astroquartz fabric bonded to aluminum with SR-585 adhesive was used as the contaminant material for the next series of tests. OCLI second surface mirrors were used as substrates. Before cementing the fabric to the aluminum, the SR-585 silicone adhesive was thinned with toluene. The bonded material was oven dried at 150°F for 5.5 hours, and then installed in the VES as a flat disc with the fabric facing the nozzle of the VES. At a source temperature of 140°C and with the substrate at -100°C, the initial deposition rate was 55Å/min, and after aging 4 hours was 8Å/min. The initial rate appeared to be very high, and was not considered representative of the system. The high rates were thought to be due to residual solvent in the adhesive.

The drying technique employed with this system was reviewed with Mr. Al Eagles of General Electric. Their procedure for bonding silica fabric was to drive off the solvent at 150°C for 3 hours under vacuum.* This procedure was adopted with a new specimen, and it showed a considerable reduction in outgassing. The initial deposition rate with this material was 18.6Å/min, and after three hours aging it was 9.8Å/min.

To determine the changes in solar absorptance, α_s , measurements were made of the substrate before contaminant deposition, at two levels of contaminant thickness, and after irradiation. The results of three separate experiments using ultraviolet radiation, electron irradiation, and proton radiation are shown in Figure 14.

*Note: SR-585 is a silicone pressure sensitive adhesive, supplied as a solution in toluene, which must be evaporated to develop the adhesive properties. The vendor data sheet recommends air drying or heating at modest temperatures (85-100°C) for solvent removal. Greater cohesive strength is claimed by curing 5-10 min. at 250°C after solvent removal, or by adding a catalyst (benzoyl peroxide) and heating the treated, solvent-free material for 5-10 min. at 150°C.

Figure 14 Solar Absorptance of SR-585 Contaminated and Irradiated Second Surface Mirror

Run No.	Film Thickness	Irradiation	α_s	Change from Initial Value
1	Clean surface	None	0.058	Initial value
	463Å	"	0.061	+5.2%
	932Å	"	0.068	+17.2%
	"	After 76 ESH UV	0.067	+15.5%
	"	After 160 ESH UV	0.069	+19.0%
2	Clean surface	None	0.063	Initial value
	458Å	"	0.062	-1.6%
	950Å	"	0.056	-12.7%
	"	10^{16} e/cm ²	0.050	-20.6%
3	Clean surface	None	0.052	Initial value
	508Å	"	0.052	No measurable change
	"	10^{16} p/cm ²	0.058	+11.5%

The irradiation fluxes were the same as used previously: 155 equivalent solar hours at 3.61 ultraviolet solar constants; 2.7×10^{12} electrons per cm² per second at 15KeV; and 8.1×10^{12} protons per cm² per second at 5KeV. Exposure time was 43 total hours for UV, 1 hour for electrons, and 20 minutes for protons.

Within any given run, the results of Figure 14 seem straightforward, but when comparing data runs there appear to be some inconsistencies in the results.

The results of Run 1 show that α_s increases with contaminant film thickness but that ultraviolet radiation in the amounts of this test has little effect. Run 2 results are just the reverse, showing that α_s decreases with increasing film thickness and with electron irradiation. Run 3 results are not consistent with either of the previous runs in that they show no film effects, but they do show a positive change in α_s after proton irradiation.

This raises obvious questions which deserve further explanation, such as:

1. Should not equal thicknesses of the same contaminant on the same kind of substrate give the same percentage change in α_s ?
2. Why does one run show a decline in α_s and another run show an increase?
3. If electron irradiation changes α_s at all shouldn't it cause an increase?

There is some scatter in the measurement, but this does not provide a sufficient answer to the questions although it undoubtedly contributes something to the difficulty of making specific judgements about the data. Note that the measured initial value of α_s for the three substrates averages about 0.058 with a deviation from this average of about $\pm 10\%$. The average agrees well with the accepted value of 0.05 for these kinds of second surface mirrors, and the accuracy of the measurement is within acceptable limits for this quantity. Thus it appears that the method is initially good, but that trying to determine the changes in α_s as a result of contamination and irradiation causes the problems.

The method chosen to determine α_s was the hemispherical reflectance method using an averaging sphere. From scans of reflectivity versus wavelength, the integrated reflection of the solar spectral energy can be determined, and rationing this to the total incident solar radiation gives the fraction of radiant energy reflected and also its complement, the fraction absorbed. This procedure is fairly standard and has given good results.

However, an unexpected difficulty arose during initial tests with these combination materials. After contaminant deposition, it was observed that sample reflectivities increased with increasing film thickness. In some cases the reflectivity was greater than 100%. This obviously unrealistic result was thought to be due to the clean specular samples becoming increasingly diffuse with greater film thickness. Hence, some of the light might have been scattered directly onto the detector, and which could give an anomalously high output signal compared to the reference beam that first struck the diffuse sphere wall and became averaged. Extensive study was devoted to this problem by considering the symmetry of the relationship among the detector locations, the reference and sample beams, and the area on the sphere wall where the specularly reflected sample beam would fall. From this study it was determined that several changes in geometry would

improve the compatibility of the sphere to accept both specular and diffuse samples. Modifications were made to the detector locations on the sphere surface and to baffles within the sphere volume. These changes eliminated the anomalously high reflectances while retaining the degrees of absolute measurement and accuracy stated above.

With the improved integrating sphere the testing resumed, providing the data shown here.

The thickness of contaminant from SR-585 was determined by the frequent insertion of a QCM into the molecular beam of contaminant and measuring the flux rate at that period of time. The total accumulation on the SSM was estimated by integrating the flux rate over the total exposure period. The empirical equations of the QCM rate data determined by least squares analysis were:

$$\beta = 15.2e^{-0.0049t} \quad (15)$$

$$\beta = 26.8e^{-0.0075t} \quad (16)$$

where β = deposition rate $\text{\AA}/\text{min}$

t = time, minutes

The first equation is for the deposition prior to the UV exposure, and the second equation prior to the electron irradiation. The correlation coefficients were 0.999 and 0.989, respectively. These rates, it should be noted, were obtained with a VES which had five times the orifice area of that used in Reference 1.

The measurement of the change in the solar absorptance of contaminated specular materials introduced new problems in measurement technique, and which were solved during this program. The problem arises due to the fact that specular reflecting materials coated with a film of contaminant can become partially diffuse. This was already known from past experiments with ellipsometry when it was learned that scattering of the visible beam prevented accurate measurements for films thicker than 250\AA or so. (IR ellipsometry was developed for the purpose of circumventing this situation.) However, it was not known until now that this change in character from specular to partially diffuse would affect the ability to use standard techniques to measure the solar absorptivity, α_s . This does not suggest

that the averaging sphere technique should be abandoned totally. Indeed, the scattering measurement results discussed in the next section show that the scattering is not Lambertian, as might be assumed, but they show the scattering is sharply peaked without simple definition. Thus, bidirectional reflectance techniques, including scanned-wavelength ellipsometry, cannot be used with confidence to measure α_s because the exact nature of scattering must be known, not merely assumed, in order to account for all sources of light loss. What should be done is to adjust the sphere geometry and operating procedures accordingly. The present accuracy of ± 0.005 is quite good for measuring this quantity, and all that remains is to improve the technique to account for the specular-to-diffuse change in the sample.

B. Scattering Measurements On Contaminated Specular Reflectors

The ability of a sensor to detect a low radiance source in the presence of an intense off-axis source is limited, in part, by the off-axis energy scattered from the sensor primary mirror. Contamination of such optical surfaces can cause such scattering and impair their performance. If the contamination on an optical surface were to buildup in an optically smooth homogeneous layer, its effect could undoubtedly be predicted by the classical optical equations. However, the evidence to date indicates that contamination condensed on surfaces tends to agglomerate and produce optically nonhomogeneous coatings which introduce nonisotropic scattering which to-date does not have simple definition. The presence of particulate matter on an optical surface can produce a similar effect.

Studies were conducted as a part of this task to determine the extent of scattering caused by contamination from the two multilayer insulations, and a nonreflective black paint (Westinghouse M3221HV). All of these materials are in close proximity to the optics of a space sensor system. The measurements were made on a silver front-surface mirror with an 800-1000Å coating of SiO. The specific mirror material was not of consequence for the reflectance measurements, but its identity was necessary to insert the proper optical constants in the ellipsometer equation for estimating the thickness of the contaminant.

1. Measurement Technique

The optical arrangement for measuring the angular distribution of light reflected by contaminated mirrors is shown in Figures 15 and 16. The system consisted of a He-Ne laser ($\lambda = 0.6328 \mu\text{m}$) and a variable beam expander mounted on one arm of a goniometer, and a detector system for measuring the reflected light intensity mounted on the other arm. An iris diaphragm mounted in front of the collection lens was used to control the collection angle.

The system was calibrated by moving the goniometer arms into the straight-through position, and replacing the mirror specimen with a precision optical attenuator. This type of attenuator consists of a train of three polarizers, with the first and third in a fixed, parallel orientation. The optical attenuation is then varied by rotating the central polarizer and which follows a $\cos^4 \theta$ law. The total attenuation range of the attenuator was 0 to -50 db, where

$$\text{db} = 10 \log \left(\frac{I}{I_0} \right)$$

and I and I_0 are the attenuated and unattenuated intensities, respectively. The detector output was then calibrated in terms of optical attenuation. After calibration, the goniometer arms were returned to their standard positions, with the angle of incidence of the laser beam on the sample mirror fixed at 25° from normal to the mirror.

The intensity measurement techniques were modified slightly when the mirror (clean and contaminated) was used with the Westinghouse black paint. For Insulations No. 1 and No. 2, the clean mirror was scanned with the goniometer with an iris diameter of 0.02 in. (beam distance from source to iris was 12.60 in.). For the lower levels of scattered energy, the iris was opened to 0.95 in. diameter, with no change in detector current measurement scale range. This reduced problems with detector linearity, but also reduced the range of measurement at each iris setting; at the high sensitivity setting (large iris diameter), which gave good results of scattered energy at angles greater than $\pm 2^\circ$ from the specular angle of reflection, details of the peak itself were lost. At the low sensitivity iris setting, the peak was well defined, but provided low resolution of the low intensity scattered radiation.

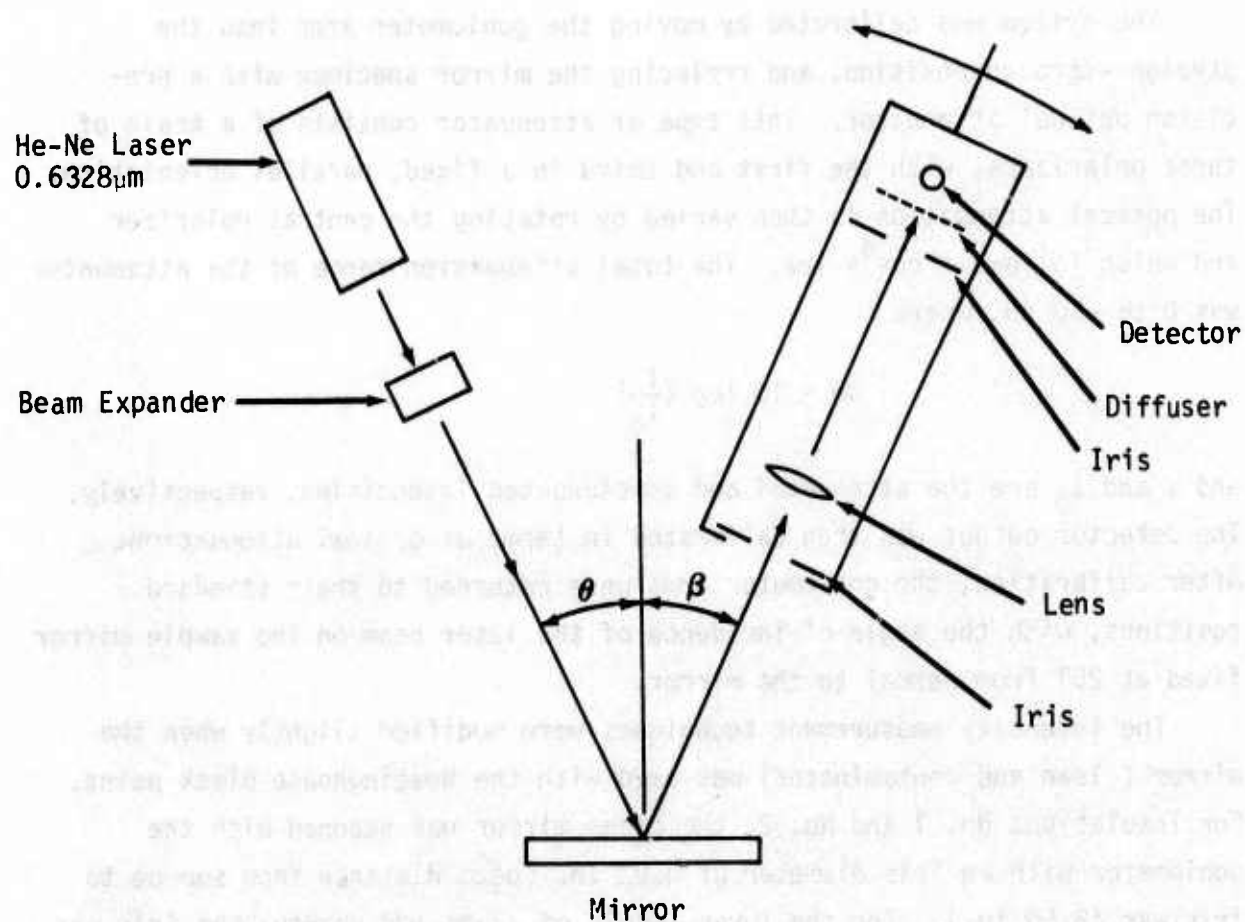


Figure 15 Laser-Goniometer System for Scattering Measurement

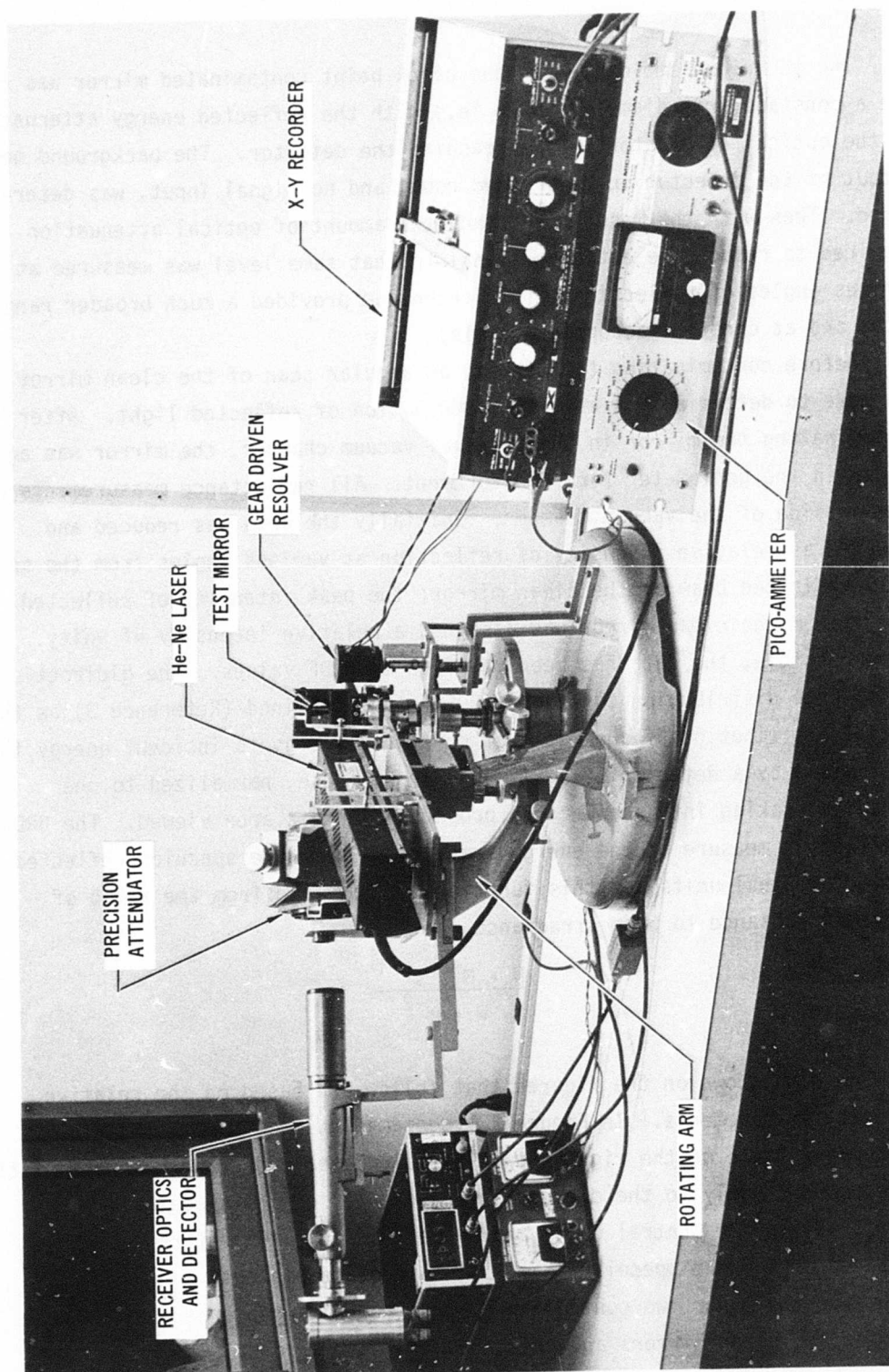


Figure 16 Laser-Goniometer Scattering Measurement

12-8386-1

The technique employed with the black paint contaminated mirror was to use a constant iris diameter (0.35 in.) with the reflected energy attenuated by the optical attenuator before reaching the detector. The background noise output of the detector in a darkened room, and no signal input, was determined. Then with the laser operating, the amount of optical attenuation required to reduce the detector signal to that same level was measured at various angles of reflection. This technique provided a much broader range of data, and at constant acceptance angle.

Before contaminating the mirror, an angular scan of the clean mirror was made to determine its angular distribution of reflected light. After contaminating the mirror in the trilevel vacuum chamber, the mirror was again placed in the goniometer for remeasurement. All reflectance measurements were made outside of the vacuum chamber. Initially the data was reduced and reported as relative intensity of reflection at various angles from the specularly reflected beam of the clean mirror; the peak intensity of reflected energy from the clean mirror was assigned a relative intensity of unity. Where possible, the data has been modified to BRDF values. The bidirectional reflectance distribution function (BRDF) can be defined (Reference 3) as the spatial distribution of the ratio of scattered energy to incident energy that is observed by a detector of small angular subtense, normalized to one steradian, taking into account the projected surface area viewed. The BRDF is, in effect, a measure of the energy scattered out of the specular reflected beam. The usual units for this function are obtained from the ratio of reflected radiance to beam irradiance, or

$$\frac{W \cdot M^{-2} \text{ sr}^{-1}}{W \cdot M^{-2}}$$

The data shown on the figures that follow are based on the relative intensity measurements. In Figure 22 (contaminant from the black paint) a secondary scale on the right shows the calculated BRDF. However, the latter values do not apply to the curve within about $\pm 2^\circ$ of the specular beam as that is within the central beam, and by definition, BRDF refers to energy scattered out of the specular beam. It was not feasible to calculate BRDF values for the other two contaminants as different acceptance angles were used for the clean mirrors and the contaminated mirrors.

2. Scattering Results

(a) Insulation No. 1 - This insulation, consisting of multiple layers of aluminized Kapton/glass scrim, aluminized Mylar and nylon netting was deposited with the VES at 140°C, and the thickness of the deposited contaminant was monitored with the ellipsometer. Thickness of the deposit was calculated on the assumption that the optical constants of the deposit would be the same as for typical organic materials (i.e., $n = 1.5$, $k = 0.0$), and on that basis, the total thickness after 2.83 hours was 303Å. However, later observations caused us to question the correctness of the assumption on optical constants.

The contaminated mirror was examined by phase contrast microscopy immediately after removal from the vacuum chamber. This examination revealed that the contaminant consists primarily of fine particles, as shown in Figure 17. The size of these particles fall into two distinct ranges, the large particles having typical dimensions of $0.6 \times 1.2 \mu\text{m}$, and small ones having typical dimensions of $<0.2 \mu\text{m}$. The latter particles are barely discernible in Figure 17, but were readily apparent in visual examination under the microscope. There appeared to be very few particles having intermediate dimensions, a likely indication that two different materials were being deposited. The particle density of the larger particles was approximately $1.86 \times 10^6/\text{cm}^2$.

The results of the light scattering measurements are shown in Figure 18, which shows the results with the mirror clean and contaminated. Noteworthy are the side lobes of scattered energy beginning at about $\pm 3.2^\circ$ from the specular beam.

It is uncertain which component of the multilayer insulation was responsible for the scattering. The contaminant appears to be particulate matter in the photomicrograph and may be flakes of the vapor deposited aluminum or debris from the nylon net or glass scrim cloth. Consequently our conclusions as to the thickness of the deposit may not be valid, as the thickness, measured ellipsometrically, was based on the optical constants for an organic material.

(b) Insulation No. 2 - Contaminant from Insulation No. 2 was deposited on the mirror over a 3-1/2 hour period with the VES at 140°C and the mirror at -20°C. Examination of the mirror by phase contrast microscopy (Figure 19) showed a

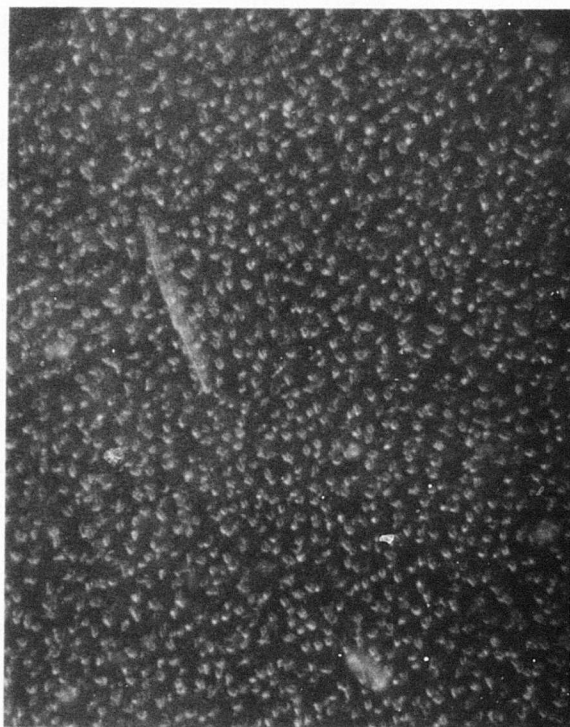


Figure 17 Contaminant from Insulation No. 1 on Silver Mirror (400X)

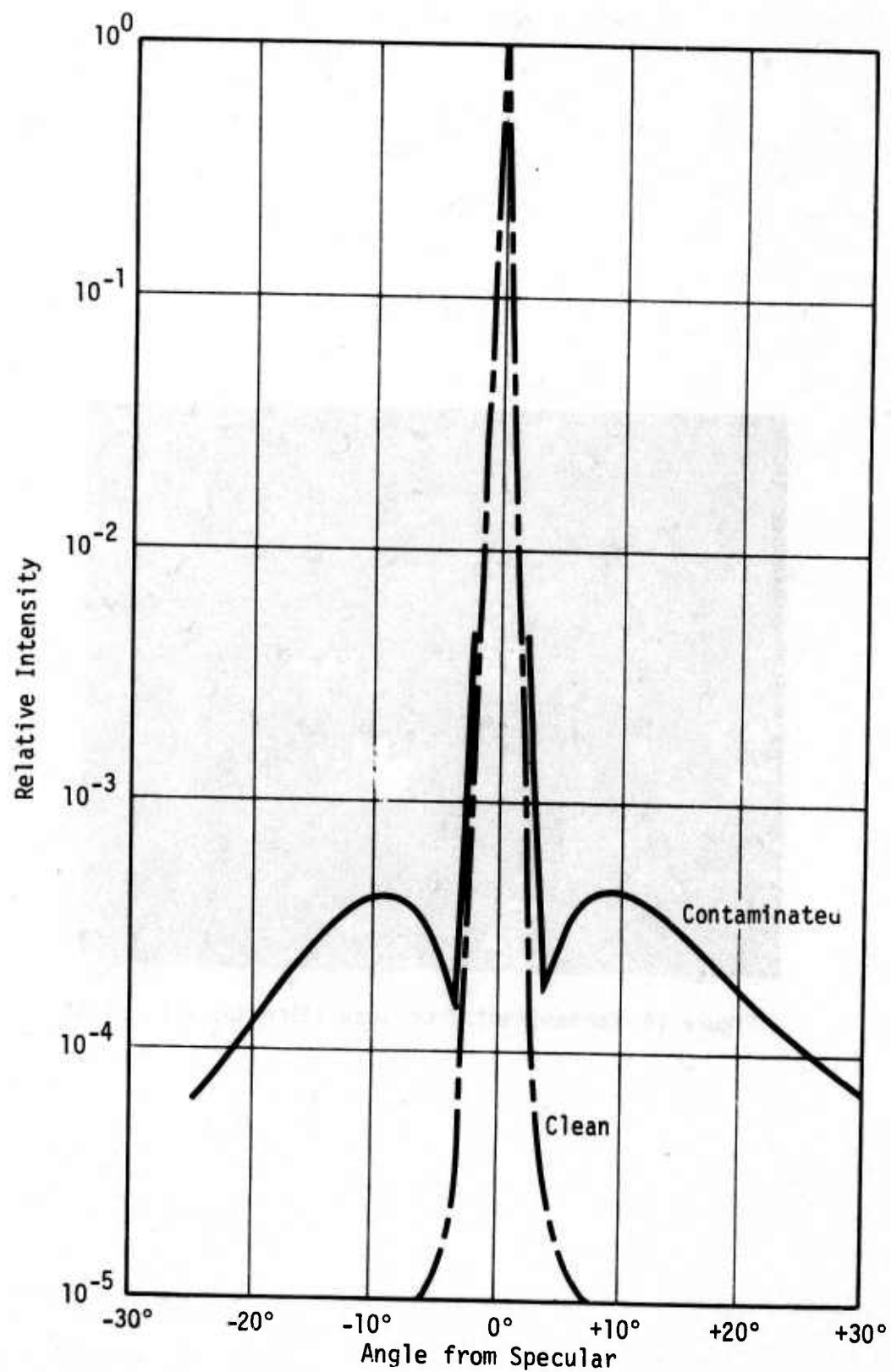


Figure 18 Scattering Due to Contamination from Insulation No. 1
($\lambda = 0.6328 \mu\text{m}$)

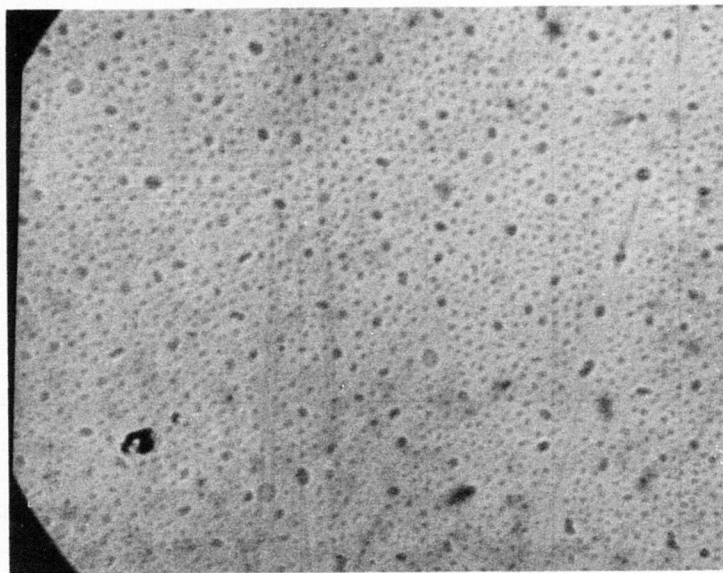


Figure 19 Contaminant from Insulation No. 2 (~550X)

broader range of particle sizes than from Insulation No. 1. However, the effect of the contaminant on scattering from this insulation was very small as shown by Figure 20, and much less than the contaminant from Insulation No. 1.

(c) Westinghouse Black Paint (Westinghouse M3221 HV) - Contaminants/ outgassing species from this black paint of unknown composition were deposited over a 30 minute period with the VES at 140°C and the mirror at -20°C. The duration of deposition was judged by visual observation of the mirror during deposition. A phase contrast photomicrograph is shown in Figure 21, and the scattering measurements in Figure 22. The scattering effects from the contaminant from the black paint were much more severe than from either of the multilayer insulation materials.

The photomicrograph (Figure 21) suggests that the contaminant is a condensed fluid rather than particulate. The light areas enclosed within dark bands are typical of agglomerates of a fluid nature. The halo around the dark band also suggests that a second fluid may also be present which forms a relatively smooth surface film in which the agglomerates are embedded.

C. Total Weight Loss and Collected Volatile Condensable Material Tests

Outgassing tests and volatile condensable material tests have been run on the materials studied under this task. These tests were run by John J. Park, Materials Engineering Branch of the NASA Goddard Space Flight Center using the standard micro-VCM test method. The outgassing tests are conducted at 125°C for 24 hours in a vacuum of 10^{-6} torr, with the condensable materials being collected at 25°C within the same system. The data reported are the Total Mass Loss and the Collected Volatile Condensable Materials (CVCN). The criteria for acceptability established by NASA is a maximum of 1.0% Total Mass Loss and a maximum of 0.10% CVCN. The outgassing results provided by Dr. Park are as follows:

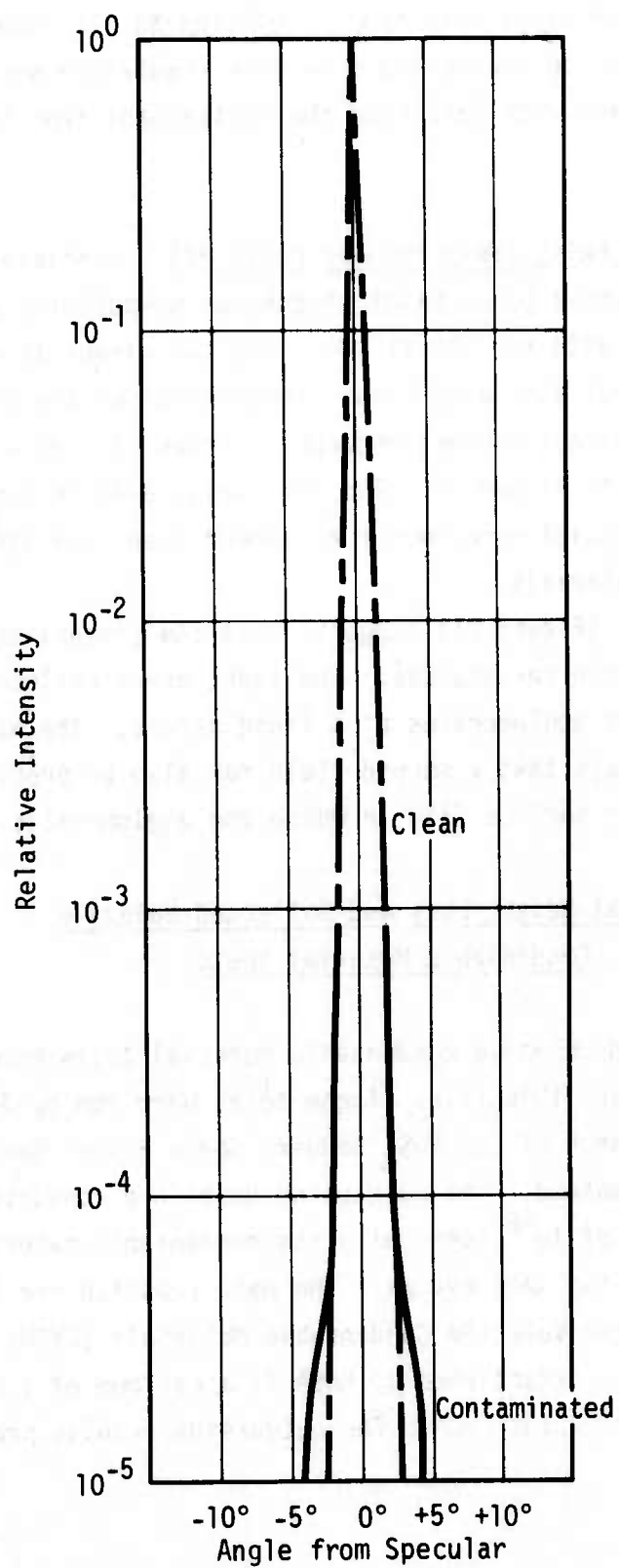


Figure 20 Scattering Due to Contamination from Insulation No. 2
($\lambda = 0.6328 \mu\text{m}$)

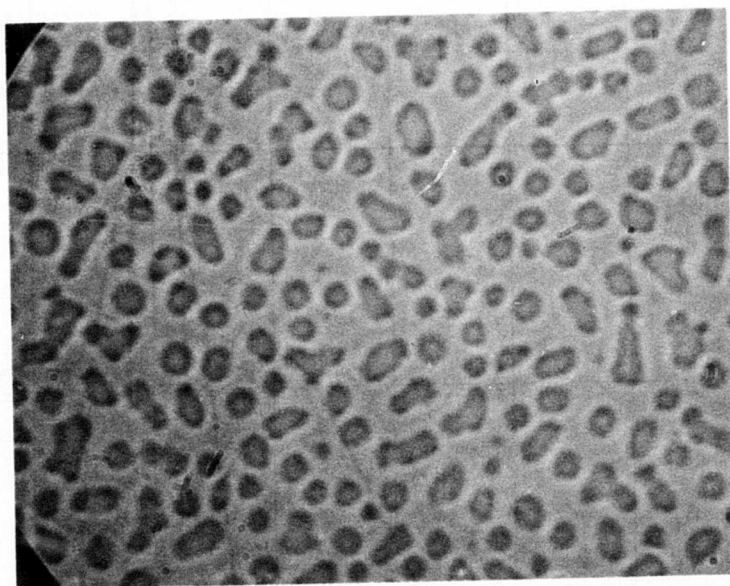


Figure 21 Contaminant from Westinghouse Black Coating (~550X)

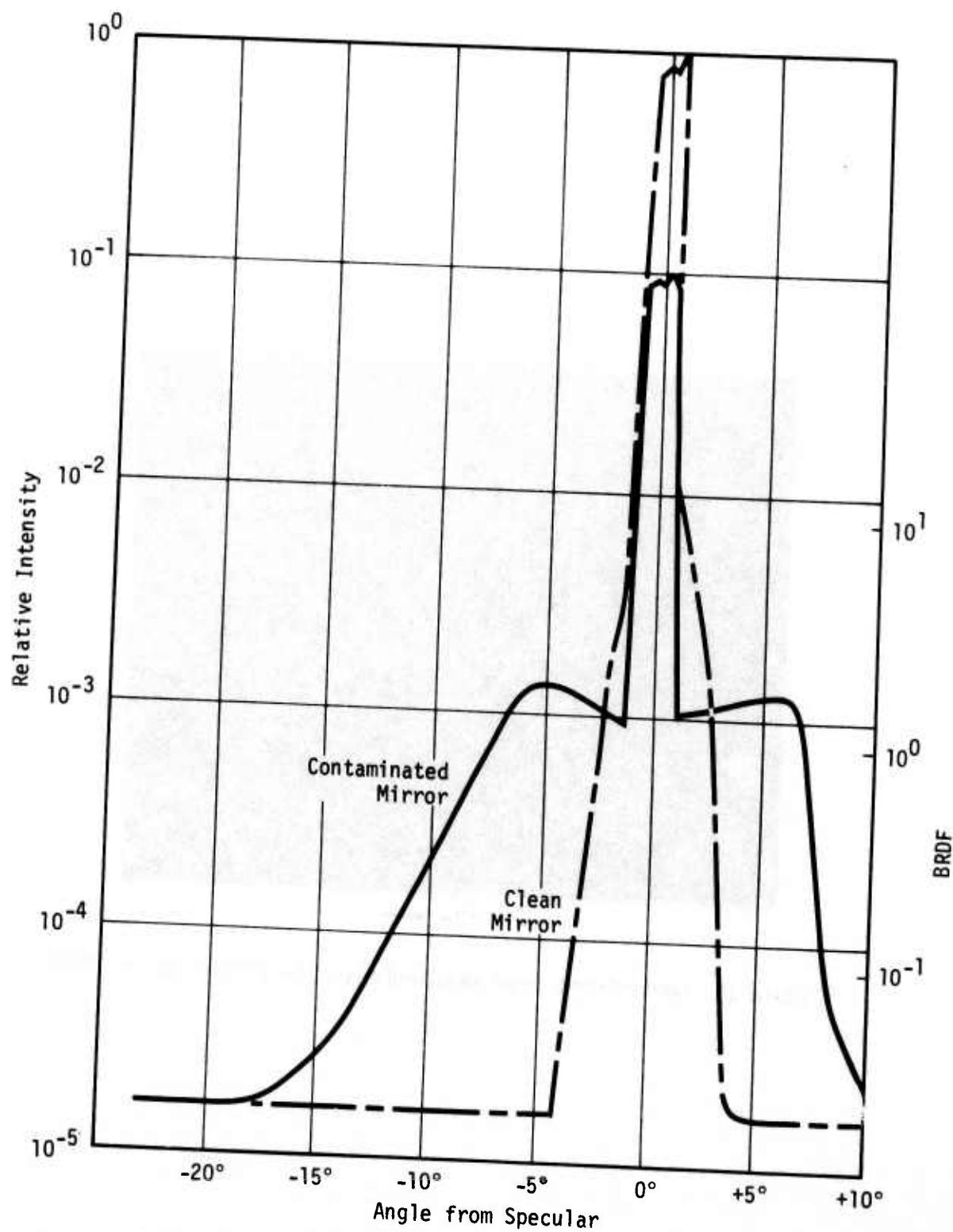


Figure 22 Scattering Due to Contamination from Westinghouse Black Coating ($\lambda = 0.6328 \mu\text{m}$)

Insulation Blanket No. 1. (GSFC 6814)

Aluminized Kapton (1 mil) reinforced with glass scrim; 10 layers of aluminum Mylar (0.25 mil) alternating with 11 layers of Nylon netting; aluminized Kapton (1 mil) reinforced with glass scrim.

Total Mass Loss 1.60%

Condensables 0.04%

Insulation Blanket No. 2. (GSFC 6812)

Aluminized Teflon (2 mil); 10 layers of aluminized Mylar (0.25 mil) alternating with 11 layers of Nylon netting; aluminized Mylar.

Total Mass Loss 0.44%

Condensables 0.00%

Astroquartz Fabric/Aluminum No. 3. (GSFC 6808)

Astroquartz fabric bonded to aluminum with AFML/Hughes Aircraft modified RTV-602. Cured at room temperature. Aluminum foil was removed before test.

Total Mass Loss 0.10%

Condensables 0.00%

Astroquartz Fabric/Aluminum No. 4. (GSFC 6810)

Astroquartz fabric bonded to aluminum with SR-585 silicone adhesive. Solvent evaporated by treating the bonded specimen at 65°C in air for four hours, plus 3 hours at 150°C in vacuum. Aluminum foil was removed before test.

Total Mass Loss 0.97%

Condensables 0.54%

In evaluating this data, it should be recognized that some of these samples were composites of mixed outgassing materials, and that some of the base weight on which the percentages were calculated included inert material.

It is noted that while only a very small amount of CVCM is reported for Insulation No. 1, it produced a significant amount of scattering (Figure 18), and that Insulation No. 2 had no measurable CVCM and negligible scattering. Also, the TWL of Insulation No. 1 exceeded the criteria established by NASA for acceptability.

The comparative results for AFML/HAC RTV-602 and SR-585 bear out the relative outgassing data measured by the VES technique.

V. TASK 3 - KINETICS OF LOW OUTGASSING MATERIALS

Several candidate materials are being considered as adhesives for woven fabric thermal control materials. One of the critical properties of such an adhesive is its outgassing rate. The candidate adhesives include RTV-566, SR-585, and the Hughes Aircraft Company modification of RTV-602. The outgassing properties of RTV-566 had been previously determined (Reference 1), but no data have been available on the other two silicones, based on the VES technique employed in this program. To provide uniformity of test conditions with the previous work, the same multiorifice nozzle was used with the VES.

A. AFML/HAC RTV-602

The purified RTV-602 was cured at room temperature with 0.2% of tetramethylguanidine (in a 5% hexane solution). The deposition was made with the VES at 140°C, with a gold coated mirror substrate at 23°C. Deposition and reevaporation rates were measured with the ellipsometer using the He-Ne laser at 6328Å wavelength.

The initial deposition rate was extremely low, requiring 32 minutes to deposit a 41Å thick film. Reevaporation of the deposited film was also very slow (about 0.6Å/min for the initial deposit), to the extent that the precision undoubtedly suffered. Two deposition and reevaporation measurements were made as described above, plus a final deposition with the substrate at -25°C. The latter indicated that the sticking coefficients were approximately 0.1 at 23°C.

Based on the limited data (Figure 23), the deposition rate, β , and reevaporation rate, γ , can be described by the empirical equations:

$$\beta = 1.47 e^{-0.0080t} \quad (17)$$

$$\gamma = 0.70 e^{-0.0077t} \quad (18)$$

where $\beta, \gamma = \text{Å/min}$

$t = \text{age at } 140^\circ\text{C, minutes}$

Because of the very low rates of deposition and reevaporation, it was not feasible to get additional data points beyond 6 hours age. Consequently, the shape of the curves in Figure 23, and the empirical equations are somewhat arbitrary.

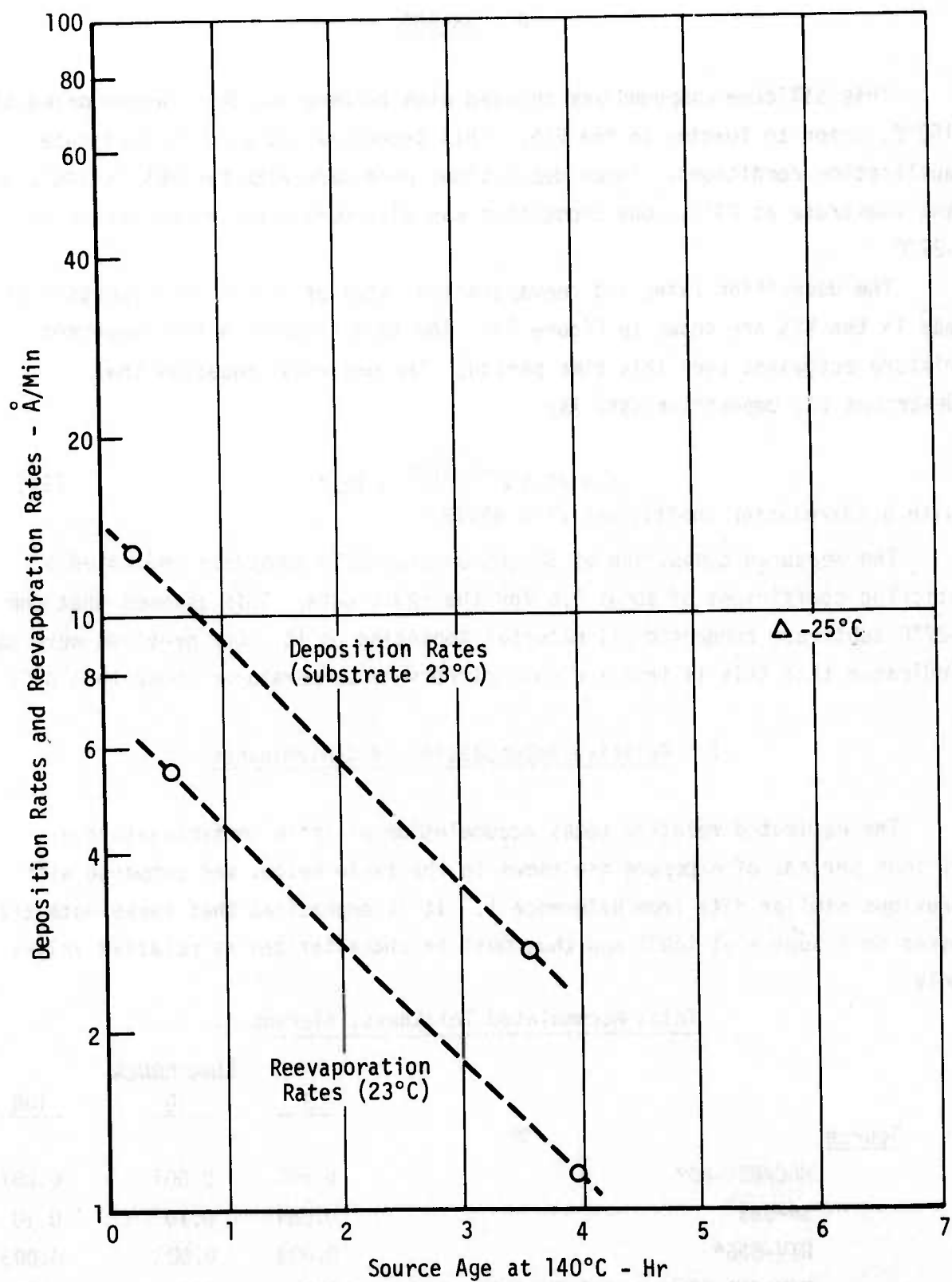


Figure 23 Deposition Rates and Reevaporation Rates of AFML/HAC RTV-602

B. SR-585

This silicone compound was thinned with toluene and then vacuum dried at 150°C, prior to loading in the VES. This procedure was used to duplicate application conditions. Three depositions were made with the VES at 140°C and the substrate at 23°C. One deposition was also made with the substrate at -27°C.

The deposition rates and reevaporation rates of SR-585 as a function of age in the VES are shown in Figure 24. The data suggests a two-component mixture outgassed over this time period. The empirical equation that describes the deposition data is:

$$\beta = 47.1 e^{-0.017t} + 10.7 \quad (19)$$

with a correlation coefficient of 0.999997.

The measured deposition of SR-585 on the -27°C substrate indicated a sticking coefficient of about 0.6 for the +23°C data. This assumes that the -27°C substrate condensed all material impinging on it. Our previous work has indicated that this is true for gold mirrors at temperatures lower than 0°C.

C. Relative Accumulation of Contaminants

The estimated relative total accumulation of these contaminants over various periods of exposure are shown in the table below, and compared with previous similar data from Reference 1. It is emphasized that these data are based on a source at 140°C and thus must be characterized as relative values only.

<u>Source</u>	<u>Total Accumulated Thickness, Microns</u>		
	<u>1</u>	<u>10</u>	<u>100</u>
HAC/RTV-602	0.003	0.007	0.007
SR-585	0.064	0.10	0.10
RTV-566*	0.003	0.003	0.003
RTV-602 (Commercial Grade)	3.2	4.28	5.62

*Source at 250°C

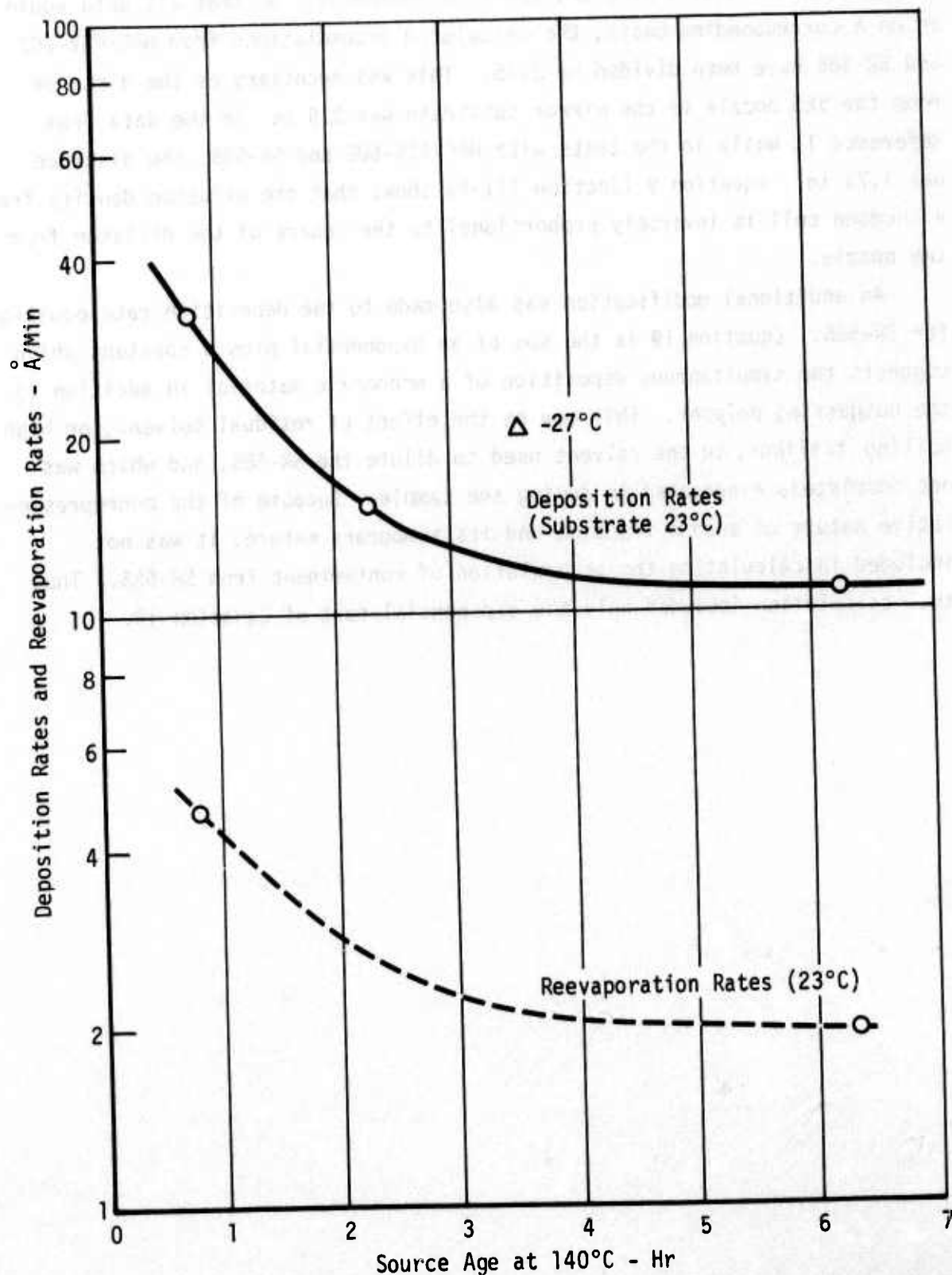
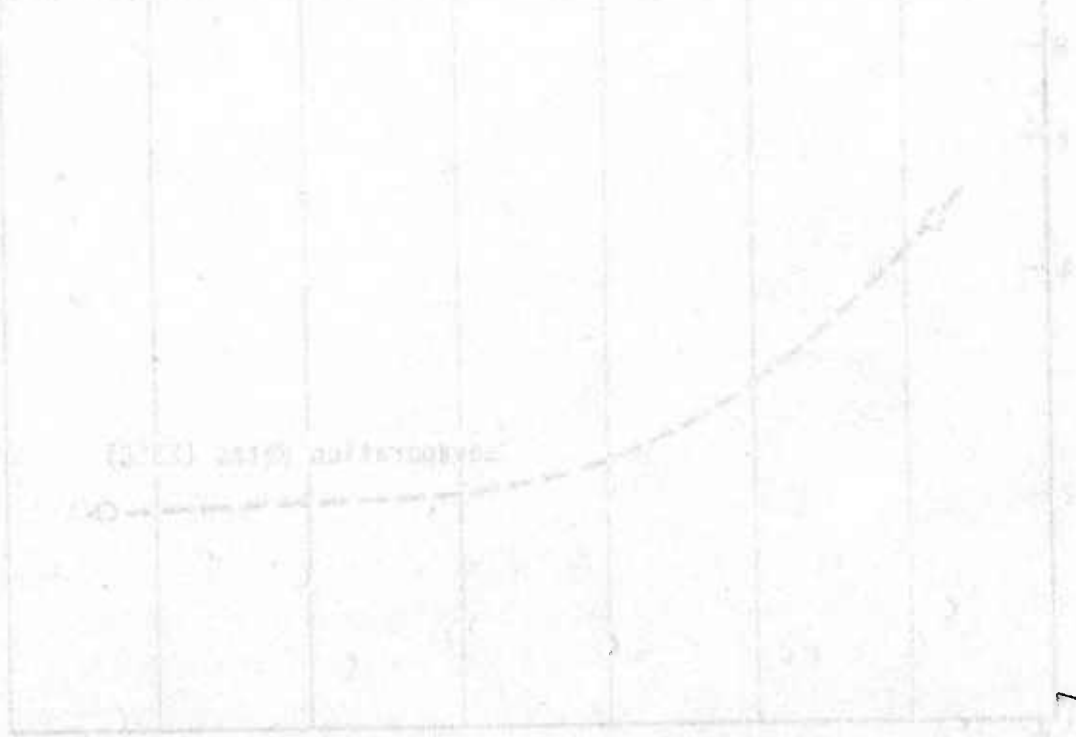


Figure 24 Deposition Rates and Reevaporation Rates of SR-585

The total accumulated thicknesses were obtained by integrating the rate equations between time zero and the time indicated. So that all data would be on a corresponding basis, the calculated accumulations from HAC/RTV-602 and SR-585 have been divided by 2.75. This was necessary as the distance from the VES nozzle to the mirror substrate was 2.9 in. in the data from Reference 1, while in the tests with HAC/RTV-602 and SR-585, the distance was 1.75 in. Equation 9 (Section III-B) shows that the effusion density from a Knudsen cell is inversely proportional to the square of the distance from the nozzle.

An additional modification was also made to the deposition rate equation for SR-585. Equation 19 is the sum of an exponential plus a constant which suggests the simultaneous deposition of a monomeric material in addition to the outgassing polymer. This may be the effect of residual solvent, or high boiling tailings, in the solvent used to dilute the SR-585, and which was not completely evaporated in drying the sample. Because of the nonrepresentative nature of such a fraction and its temporary nature, it was not included in calculating the accumulation of contaminant from SR-585. Thus that calculation included only the exponential part of Equation 19.



VI. TASK 4 - SELECTIVE REFLECTORS

A basic requirement for a low α_s/ϵ_{IR} ratio to maintain a low satellite temperature by passive means requires a high emittance (low reflectance) in the infrared band. The requirement significantly increases the vulnerability of such satellites to electromagnetic threats employing energy sources in this waveband. A potential relief from this problem might be obtained by high reflectivity over a very narrow wavelength band (centered at the threat wavelength) while maintaining high emittance over the bulk of the infrared band. One technique of achieving narrow waveband high reflectivity is through the principle of reststrahlen or selective reflectors.

Another objective of Task 4 was to examine the consequences of contamination on the dielectric stacks commonly used for enhanced transmission or reflectance of optical elements at selected wavelengths. In this study the wavelengths considered were 3.8 μm and 10.6 μm .

A. Reststrahlen Reflectors

The existence of residual rays (reststrahlen) was first discovered by E. F. Nichols in 1895, who demonstrated that crystal quartz possessed metallic reflecting power in the regions of 8.5 and 20 microns wavelength. The uniqueness of this discovery was that in these same wavelength regions quartz has pronounced absorption bands. Indeed it was later determined that there was a correspondence between the selective absorption and the selective reflection. The basic equation describing the reflectivity of an absorbing material at normal incidence is (Ref. 4):

$$R_{\lambda} = \left[\frac{(n-1)^2 + (n\kappa)^2}{(n+1)^2 + (n\kappa)^2} \right]_{\lambda} \quad (20)$$

Here the complex index of refraction is defined as $\tilde{n} = n(1-i\kappa)$ and n is the index of refraction and κ is the absorption index. For transparent materials the absorption approaches zero and the equation becomes the familiar one for reflection from a front surface:

$$R_{\lambda} = \left[\frac{n-1}{n+1} \right]_{\lambda}^2 \quad (21)$$

Therefore, in spectral regions where a material may exhibit high selective absorption, the absorption index, κ , may become sufficiently large compared to $(n-1)$ that the reflectivity is considerably higher than for other wavelengths. The region of maximum absorption does not coincide exactly with the region of strongest intensity of residual rays, the former being displaced toward longer wavelengths.

The relationship that must exist between n and κ for several levels of reflectivity is shown in Figure 25.

A review of the literature on reststrahlen was made to determine if data existed on materials which would have a naturally occurring high reflectance at the principal wavelengths of interest. The principal literature sources utilized were References 4-16. Data on the reststrahlen peaks of common materials are listed in Figure 26. It will be noted that while the bulk of these peaks occur at far-infrared wavelengths that are currently of little interest to the proposed application of the technique, two materials have peaks that fall on the desired wavelength. These materials are single crystal SiC and single crystal BeO.

The use of SiC appears dependent on the use of single crystal (though similar properties may also be obtained through other techniques discussed below). The reflectance of polycrystalline SiC (Reference 15, and as measured in our laboratory), such as the recrystallized material (Globar heater material), does not exhibit any pronounced increase in reflectivity at the desired wavelength (the reflectivity fluctuates between 20-35% from 2 μm to 15 μm wavelength). However, the single crystal (hexagonal structure) of Reference 14 exhibits 80% or greater reflectivity from 10.4 μm to 12.5 μm , peaking at 93% at 11.1 μm . Reference 16 indicates that General Electric has been using a chemical vapor deposited SiC to achieve similar results under Contract F33615-73-C-5181.

The higher reflectivity of single crystal BeO compared to polycrystalline BeO was noted also in Reference 16. It is fairly obvious that oriented crystal structures can enhance reflectivity due to reststrahlen (and may also narrow the waveband). It is by virtue of this fact that vapor deposited materials, due to their preferred crystal orientation, can also lead to enhanced reflectivity. The relatively low reflectivity of polycrystalline SiC also suggests that there may be additional materials which would have

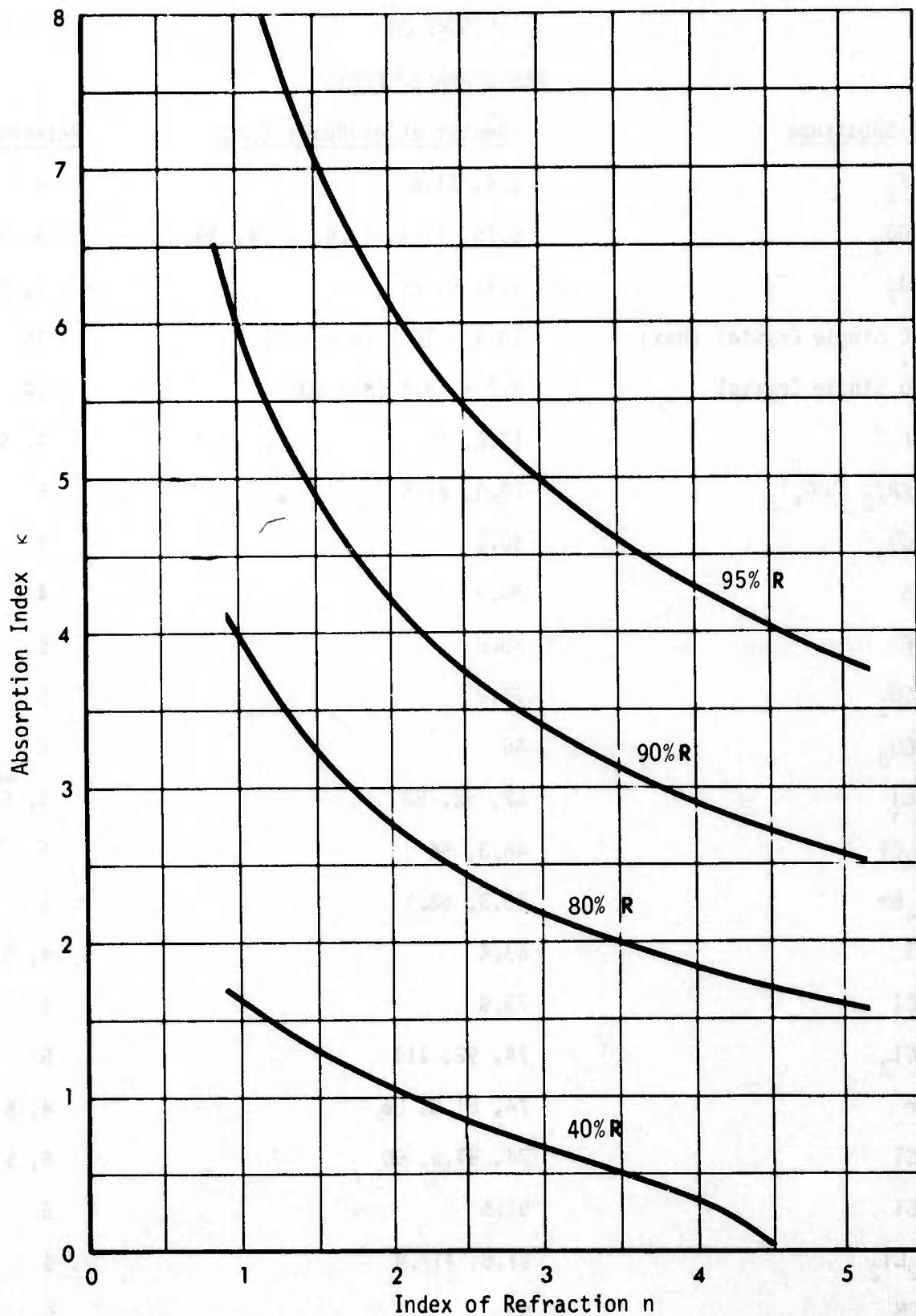


Figure 25 Relation Between Absorption Index and Index of Refraction to Obtain Various Levels of Reflectivity

FIGURE 26
RESTSTRAHLEN PEAKS

<u>Substance</u>	<u>Reststrahlen Peaks (μm)</u>	<u>References</u>
CaF_2	2.4, 31.6	4
CaCO_3	6.76, 11.4, 17.0, 29.4, 39	4, 5
SiO_2	8.4, 9, 21	4, 5
SiC Single Crystal (Hex)	10.4 - 12.5 (R > 80%)	14
BeO Single Crystal	9.7 - 13.4 (R > 80%)	14
LiF	17.0, 26	4, 5
$\text{H}_2\text{KA1}_2 (\text{SiO}_4)_3$	18.4, 21.5	5
MgCO_3	30.2	5
ZnS	30.9	4
NaF	35.8	5
SrCO_3	43.2	5
BaCO_3	46	5
NaCl	47, 52, 54	4, 5
NH_4Cl	46.3, 54	5
NH_4Br	55.3, 62.3	5
KCl	63.4	4, 5
RbCl	73.8	4
RbCl_2	74, 92, 114	5
KBr	74, 81.5, 86	4, 5
AgCl	74, 81.5, 90	4, 5
TlCl	91.6	5
Hg_2Cl_2	91.6, 117.8	5
AgCN	93	5

greatly enhanced reflectivity in controlled crystal orientation form. The search for such materials, if determined on an experimental basis, would be prohibitively expensive. However, the wavelength at which a synthesized crystal would be expected to exhibit a reflection spike could probably be calculated with the aid of quantum mechanics. The basic information needed would be the frequencies associated with the transitions between energy states, and the probabilities of those transitions when excited by energy of the specified wavelength. Under the budget allocated for this task, it was not possible to undertake detailed calculations at this time. An example of this approach is Reference 17 which describes a dispersion analysis for quartz.

B. Contamination of Dielectric Stacks

Certain optical systems are designed with high reflectance or transmittance in the 10.6 and 3.8 micron wavelength bands. Such properties are generally achieved with complex stacks of dielectric coatings on the exposed optical elements. Any contamination on a stacked dielectric coating adds an additional layer of dielectric material which may seriously alter the overall transmittance and reflectance of the optics in the wavelength regions of interest.

Theoretical studies were made of such changes due to contamination by using as a model a 21-layer dielectric stack designed by Honeywell, Inc. (Ref. 18) and calculating the reflectance of the overall stack when discrete layers of contaminant were added to the exposed surface. The calculation assumed that the contaminant was in the form of an optically smooth isotropic layer and that no scattering occurs. Based on our experience in measuring contaminant thickness by ellipsometry, we know that contamination does introduce scattering, and that the thickness of the contaminant film at which scattering occurs increases with wavelength. At 0.63 micron wavelength, scattering was noted beyond about 250Å film thickness, but at 1.38 micron wavelength, films 1400Å thick were free of scattering.

To compute the response of the dielectric stack with the contaminant added as an additional layer, it is necessary to know the optical constants of the contaminant at the appropriate wavelength. These were determined for silicone type contaminants using the ellipsometer. The real component of the index of refraction so determined and used in the computation were:

$$n_{3.8\mu} = 1.50$$

$$n_{10.6\mu} = 1.75$$

For the present purpose it was assumed that the absorption coefficient was zero. Infrared studies of silicones show that this is reasonably true. A finite absorption coefficient could affect the reflectance values, and also have an effect on transmittance. However, the changes due to a finite absorption coefficient would be expected to be small, considering the probable thickness of the contaminant, and likely range of absorption coefficients.

The calculated reflectances of the 21-layer dielectric stack with contaminant thicknesses from 0 to 16,000Å is shown in Figures 27 and 28. Figure 26 is for 10.6 μm wavelength and 10° angle of incidence. Figure 28 shows the results for 3.8 μm wavelength and 10° and 20° angles of incidence. (Reflectance at 10.6 μm and 20° incidence is not shown as it is essentially identical to 10° incidence).

The contamination is seen to degrade the reflectance of the dielectric stack by a maximum of about 1.5% at 10.6 μm. At 3.8 μm, however, the reflectance and transmittance are drastically affected.

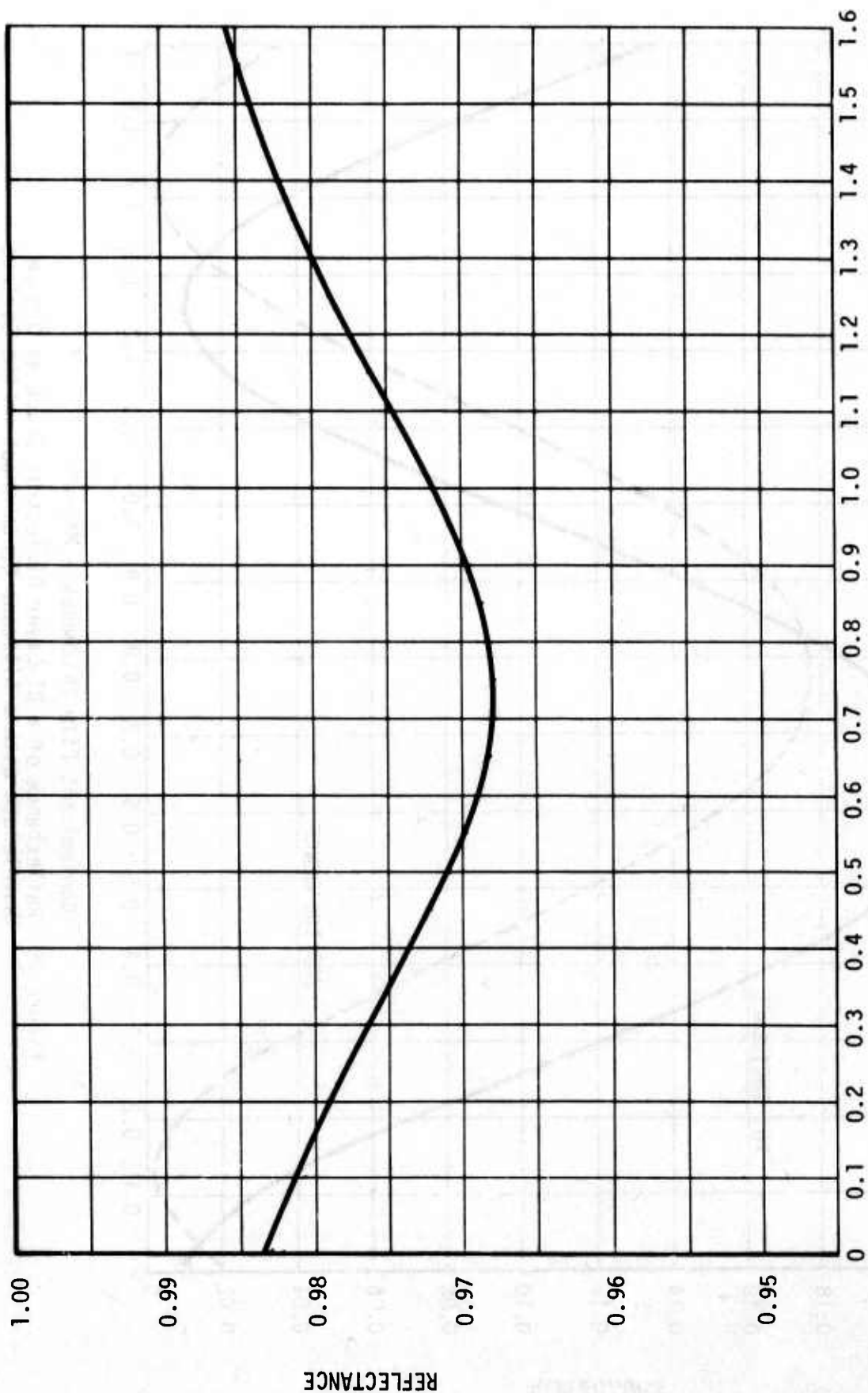


Figure 27 Reflectance of a 21-Layer Dielectric Stack at $10.6 \mu\text{m}$ Wavelength with a Silicone Contaminant on the Surface (10° Angle of Incidence)

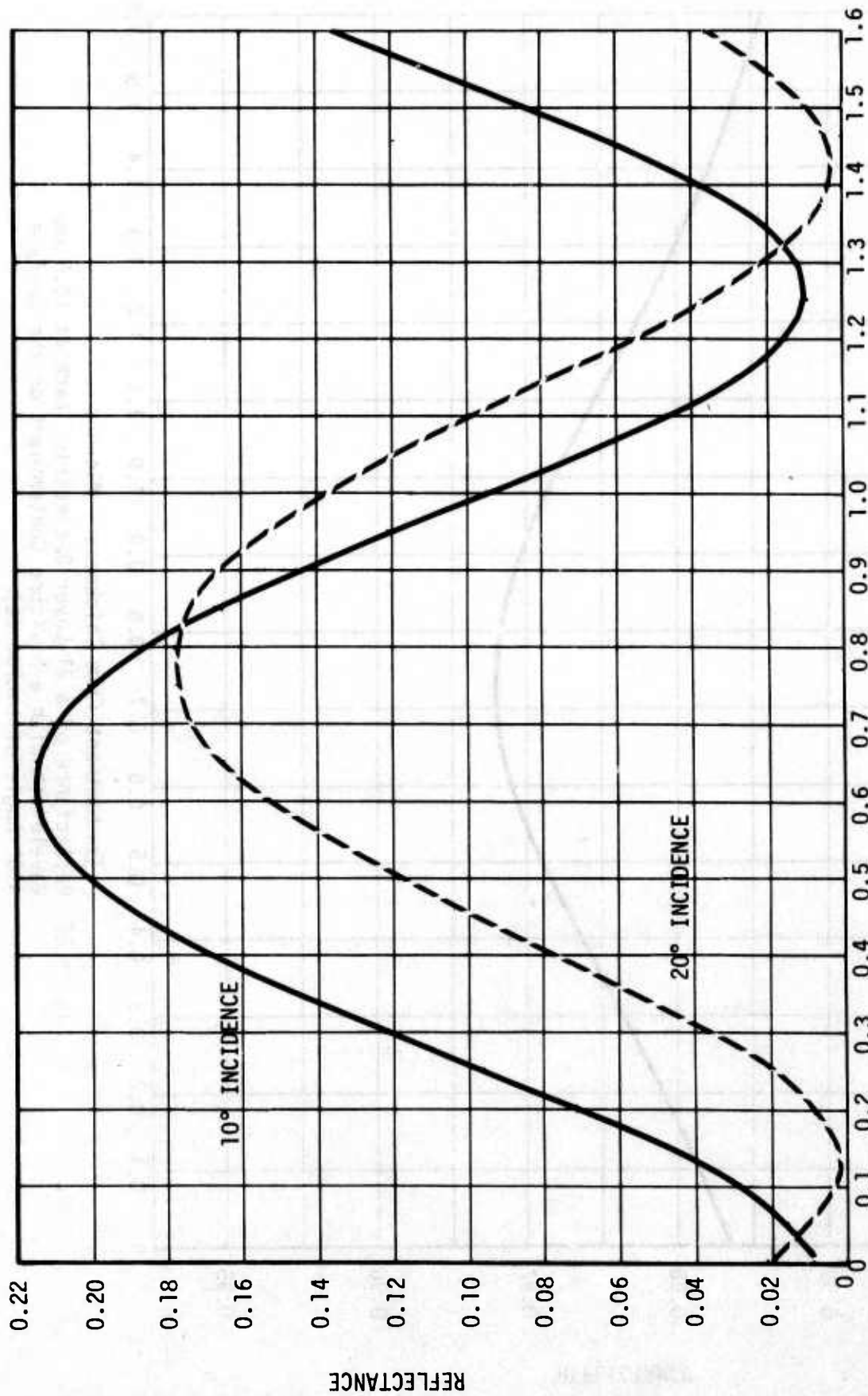


Figure 28 Contaminant Film Thickness - Microns
Reflectance of a 21-Layer Dielectric Stack at 3.8 μm
Wavelength with a Silicone Contaminant on the Surface

VII. TASK 5 - CONTAMINATION OF LASER COMMUNICATION SYSTEM OPTICS

Optical transfer of information is currently being extensively studied. Such techniques, using laser energy, frequently use multiple planes of polarization to increase the rate of data transmission, as in the projected space laser communication program. One of the technical problems that must be solved in high data rate systems is polarization mixing.

Polarization mixing is quantified as the ratio, ϵ , of the light leaked into the undesired plane of polarization divided by the light remaining in the desired plane of polarization. It is the result of imperfect conditions at reflective surfaces. Polarization mixing represents an effective degradation of the modulator performance in extinction ratio and depth of modulation. System losses due to this effect are essentially the same for all modulation formats which depend on simultaneous polarization decoding. Modulation formats which depend on nonsimultaneous polarization decoding will suffer only due to transmission caused by the leakage into the other polarization, a less severe condition. Modulation formats which do not depend on polarization decoding at all would be unaffected.

The imperfect conditions at reflective surfaces are due to large ranges of incident angles, optical surface contamination, and combinations of both. Large ranges of incident angles usually occur with gimbaled flat mirrors. While fixed mirrors can be designed with multilayer dielectric coatings to provide $\epsilon < 0.001$ for a specified angle of incidence, those mirrors which receive energy over a modest range of angles ($\sim 10^\circ$), and especially scanning mirrors which operate over a variation of 50° pose much more severe coating problems as the dielectric stack, optimized for a given angle of incidence, is detuned. The presence of contamination on the dielectric coated surface can also degrade the system by introducing or increasing polarization mixing by altering the optical characteristics of the dielectric stack.

It can be shown that the polarization mixing coefficient, ϵ , can be expressed as:

$$\epsilon = \frac{1 + (R_p/R_s) - 2(R_p/R_s)^{0.5} \cos \Delta}{1 + (R_p/R_s) + 2(R_p/R_s)^{0.5} \cos \Delta} \quad (22)$$

and

$$\epsilon = \frac{1 + \tan^2 \Psi - \tan \Psi \cos \Delta}{1 + \tan^2 \Psi + \tan \Psi \cos \Delta} \quad (23)$$

where:

- R_p = reflectivity of light in the p-plane (parallel to the angle of incidence)
- R_s = reflectivity of light in the s-plane (perpendicular to the angle of incidence)
- $R_s/R_p = \tan^2 \Psi$
- Δ = relative phase shift upon reflection experienced by the s- and p- components
- Ψ = change in reflected amplitude of the electric field vectors.

The specific value of ϵ will vary for different angles of incidence.

A. Experimental Technique

The values of Δ and Ψ can be readily obtained by use of the ellipsometer - this is the same data used for determining thickness of contaminating films on metallic mirrors. However, our previous work with the ellipsometer was at an angle of incidence of 70°. For polarization mixing, data at 45° angle of incidence was desired to reflect typical conditions. Accordingly, the ellipsometer vacuum chamber optical ports were modified to accommodate the change to 45° angle of incidence, and the compensator of the ellipsometer was recalibrated.

The experimental technique used to measure polarization mixing was to deposit contaminant from the potential source, using the vapor effusion source at 140°C on a mirror at ambient temperature in the ellipsometer-vacuum chamber. The ellipsometer data, using an He-Ne laser at 0.6328 μm wavelength, provided valid data on rate of contaminant deposition up to a total accumulation of about 200Å. While the deposition was continued well beyond that thickness, the thickness greater than 200Å had to be estimated by linear extrapolation of the initial deposition rate. Previous experience with contaminants of the general type used here has demonstrated linear deposition rates over short

periods of time. The $0.6328\text{ }\mu\text{m}$ wavelength ellipsometer data could not be used for thickness information above 200\AA because the Δ and Ψ values no longer track properly for the known optical constants of the contaminant. This is believed due to nonhomogenous films resulting in scattering at the greater thicknesses, and which lead to spurious ellipsometer data. This effect was successfully avoided in our other thick film work by using a longer wavelength laser energy source. However, in this study the use of $0.6328\text{ }\mu\text{m}$ wavelength was dictated by the need for the polarization mixing data to be obtained at a wavelength close to $0.53\text{ }\mu\text{m}$. The failure of the thicker films to track the expected Δ and Ψ relationships for thickness did not impact the use of that data for polarization mixing, as the ellipsometer was measuring the actual reflectance (regardless of whether it was affected by contaminant thickness or scattering) in the two planes of polarization in the real world at the surface of the mirror.

Two types of mirrors were employed in these tests: a plain gold mirror (vapor deposited gold on a fused silica base), and two multilayer dielectric stack coated mirrors. The dielectric coated mirrors that will ultimately be used in a laser communication system will have a very complex stack design, and are currently very rare. We used relatively simple designs that were not necessarily optimum for minimizing polarization mixing. The two dielectric stacks used here were a three-layer and a five-layer design intended to provide maximum reflectance at $0.65\text{ }\mu\text{m}$ wavelength. Quarter-wave optical thicknesses of chiolite ($5\text{NaF}\cdot 3\text{AlF}_3$) and ceric oxide were deposited in alternating layers on a gold mirror, with the high index of refraction material as the first and last coating in each design.

B. Results

The effects of contamination on polarization mixing were determined for contaminants from two sources, RTV-106 and RTV-560 silicones. Both of these materials have been tentatively selected for use in areas in close proximity to the laser communication optical system.

Results with the contaminated gold mirror are shown in Figures 29 and 30, in which the measured polarization mixing, ϵ , is plotted as a function of contaminant film thickness. The initial test indicated that the polarization mixing might be a periodic function as the thickness of the contaminant increased and which was confirmed with RTV-560 (Fig. 30).

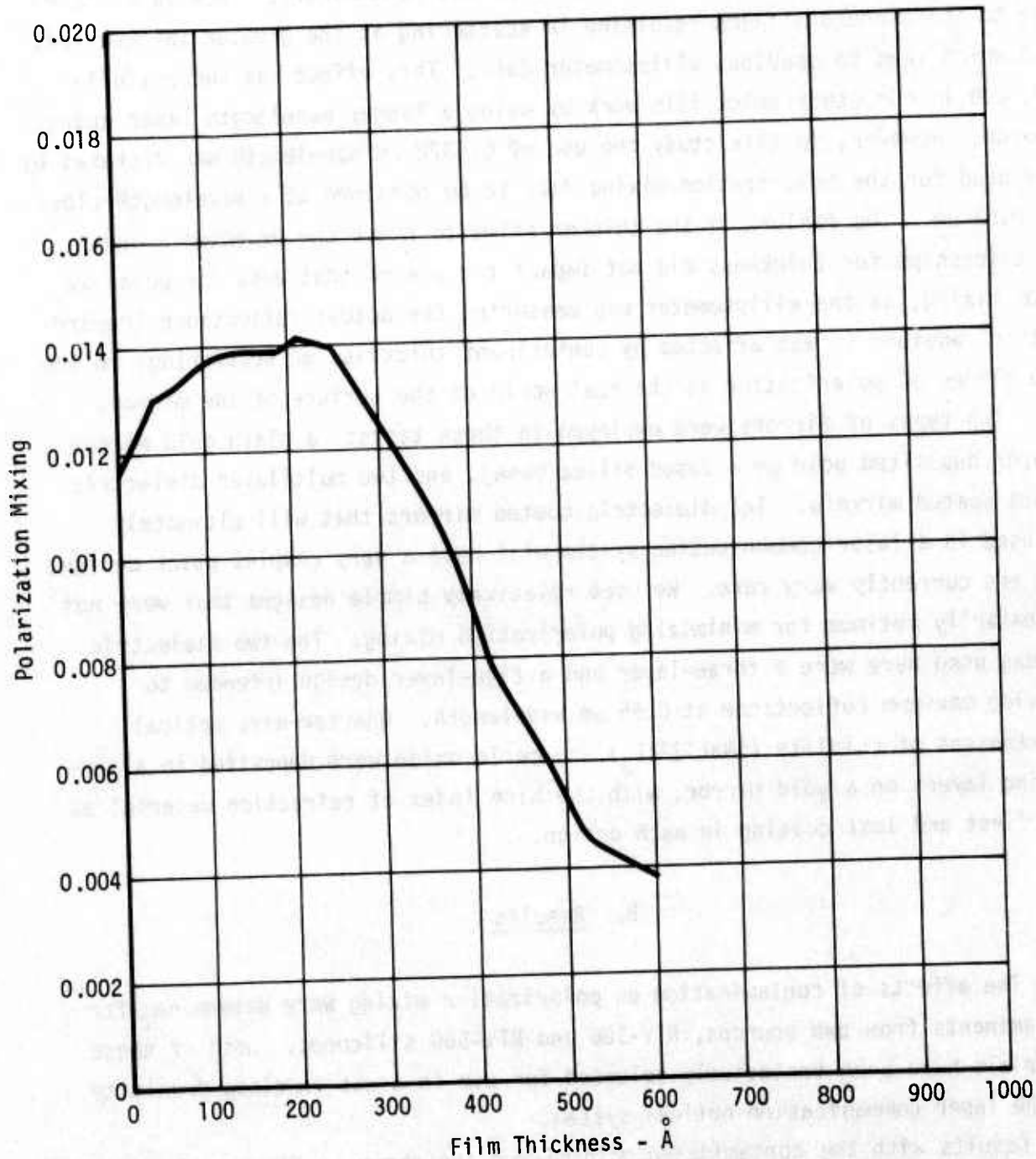


Figure 29 Polarization Mixing as a Function of Contaminant Thickness. RTV-106/Gold Mirror

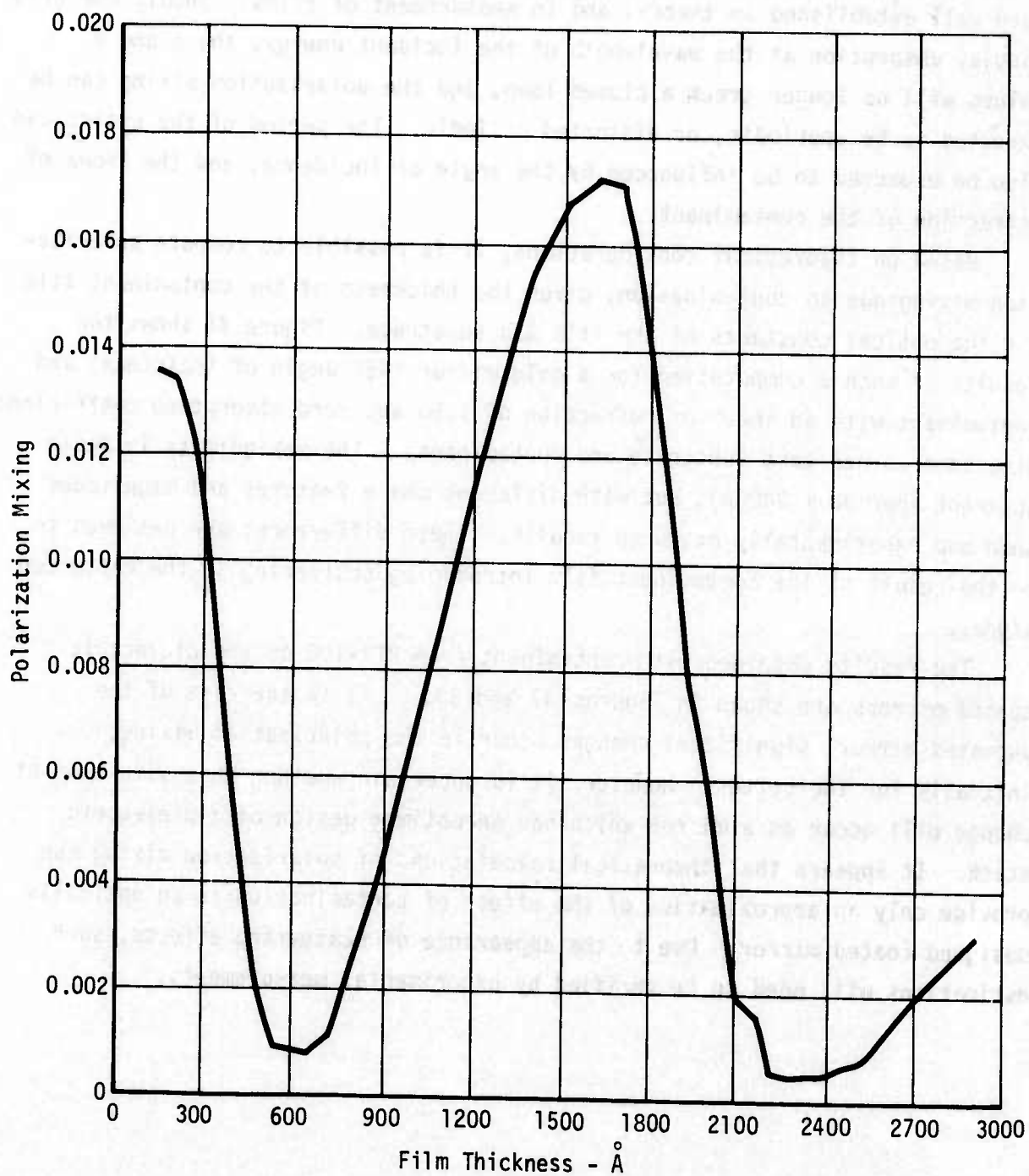


Figure 30 Polarization Mixing as a Function of Contaminant Thickness. RTV-560/Gold Mirror

The periodicity may be anticipated for nonabsorbing films on the basis that the ellipsometer Δ and Ψ values form a closed loop, and all values will eventually repeat themselves as the thickness of the film increases. This has been well established in theory, and in measurement of films. Should the film display absorption at the wavelength of the incident energy, the Δ and Ψ values will no longer track a closed loop, and the polarization mixing can be expected to be aperiodic, or distorted periodic. The period of the cycles can also be expected to be influenced by the angle of incidence, and the index of refraction of the contaminant.

Based on theoretical considerations, it is possible to compute polarization mixing due to contamination, given the thickness of the contaminant film and the optical constants of the film and substrate. Figure 31 shows the results of such a computation for a gold mirror (45° angle of incidence) and contaminant with an index of refraction of 1.50 and zero absorption coefficient (the same as our test substrate and contaminant). The periodicity is again apparent (period $\sim 2400\text{\AA}$), but with different shape features and magnitudes than our experimentally measured results. These differences are believed to be the result of the contaminant film introducing scattering in the reflected signal.

The results obtained with contaminant from RTV-106 on the dielectric coated mirrors are shown in Figures 32 and 33. As in the case of the uncoated mirror, significant changes occur in the polarization mixing, initially for the better. However, it is uncertain whether this same mode of change will occur on a mirror which has an optimum design of a dielectric stack. It appears that theoretical calculations of polarization mixing can provide only an approximation of the effect of contamination on an optimally designed coated mirror. Due to the appearance of scattering effects, such estimations will need to be verified by experimental measurements.

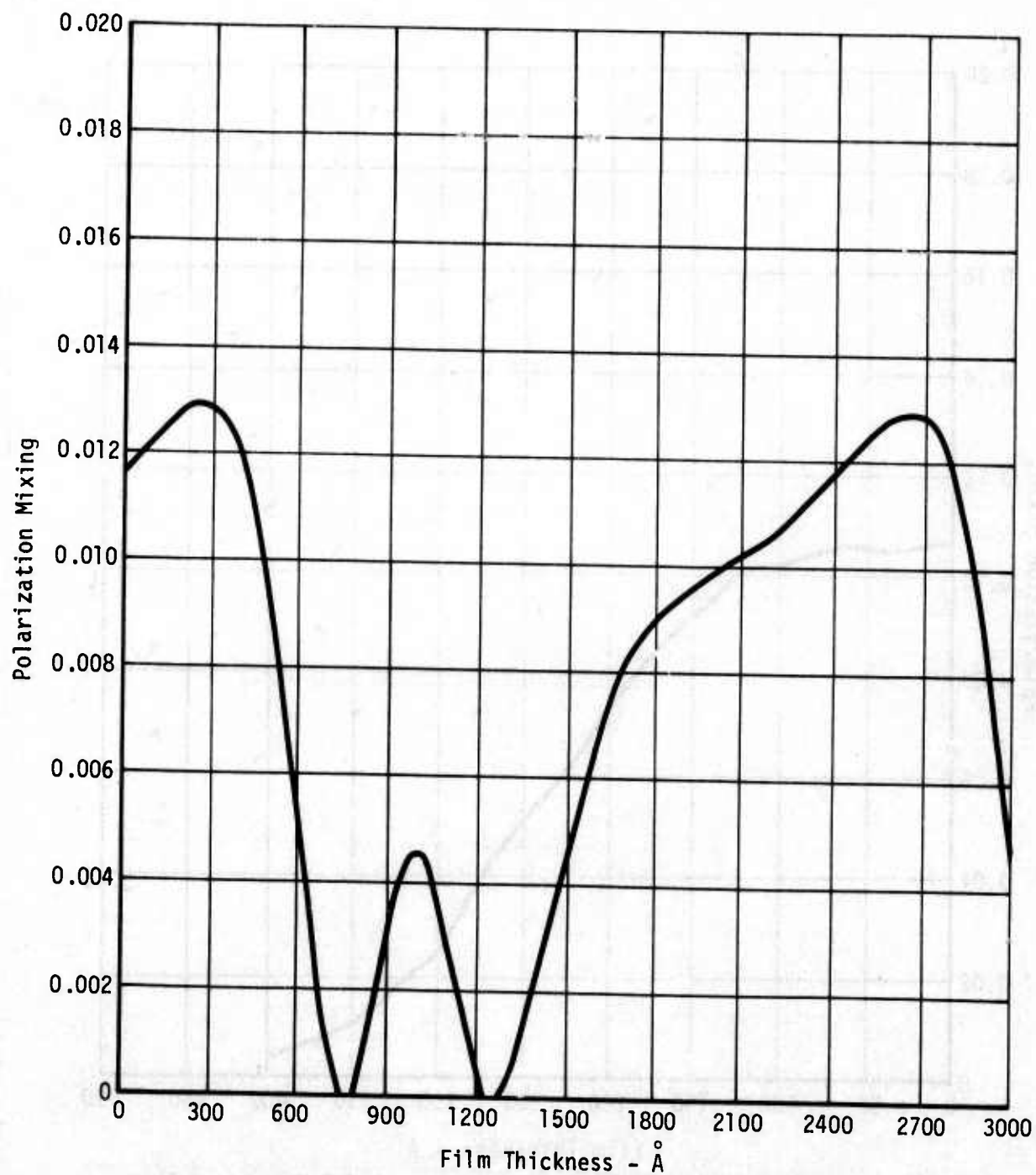


Figure 31 Calculated Polarization Mixing Due to an Organic Film on a Gold Mirror $n = 1.50$, $k = 0.0$

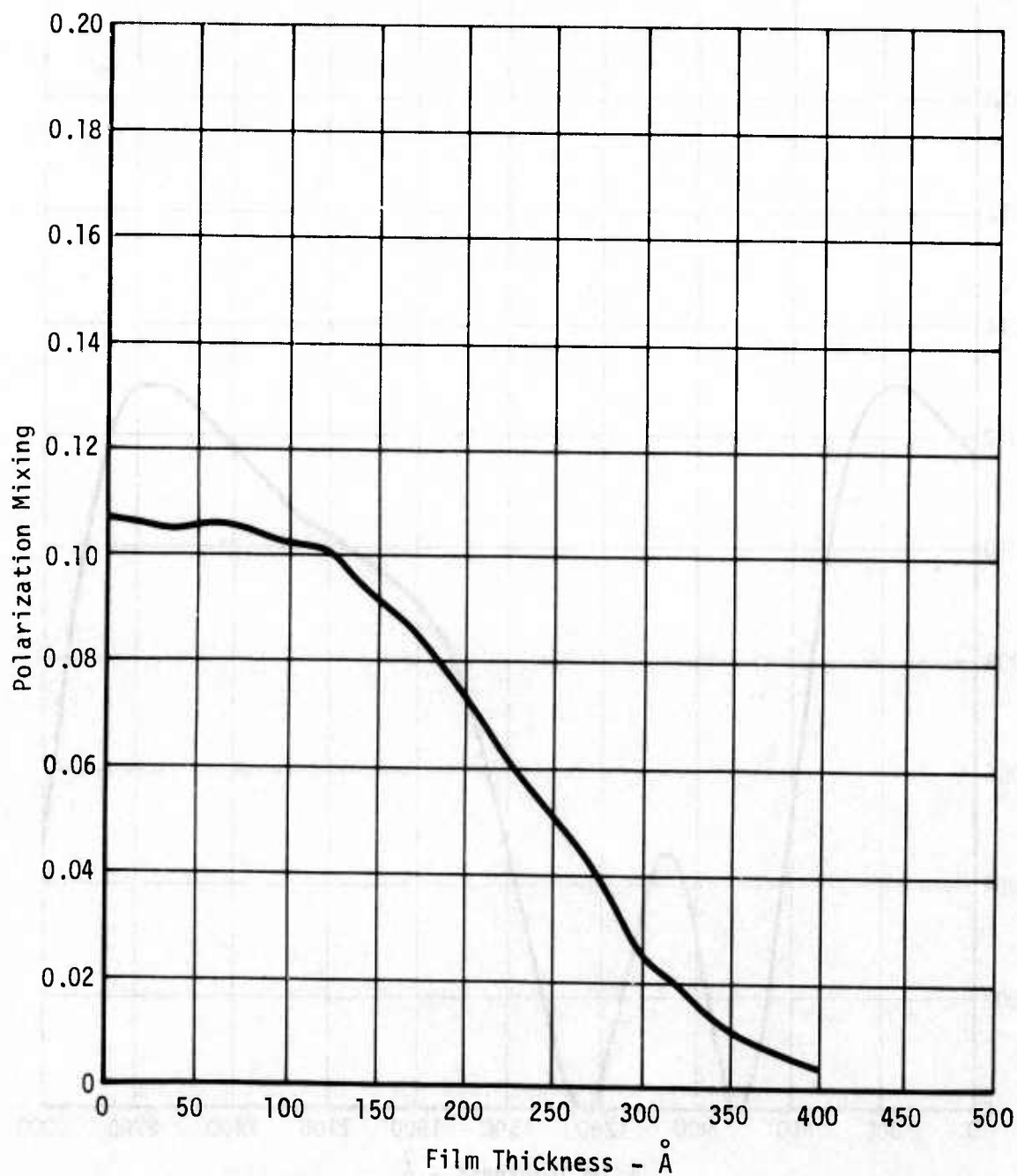


Figure 32 Polarization Mixing as a Function of Contaminant Thickness. Three Layer Dielectric Stack on a Gold Mirror. Contaminant from RTV-106

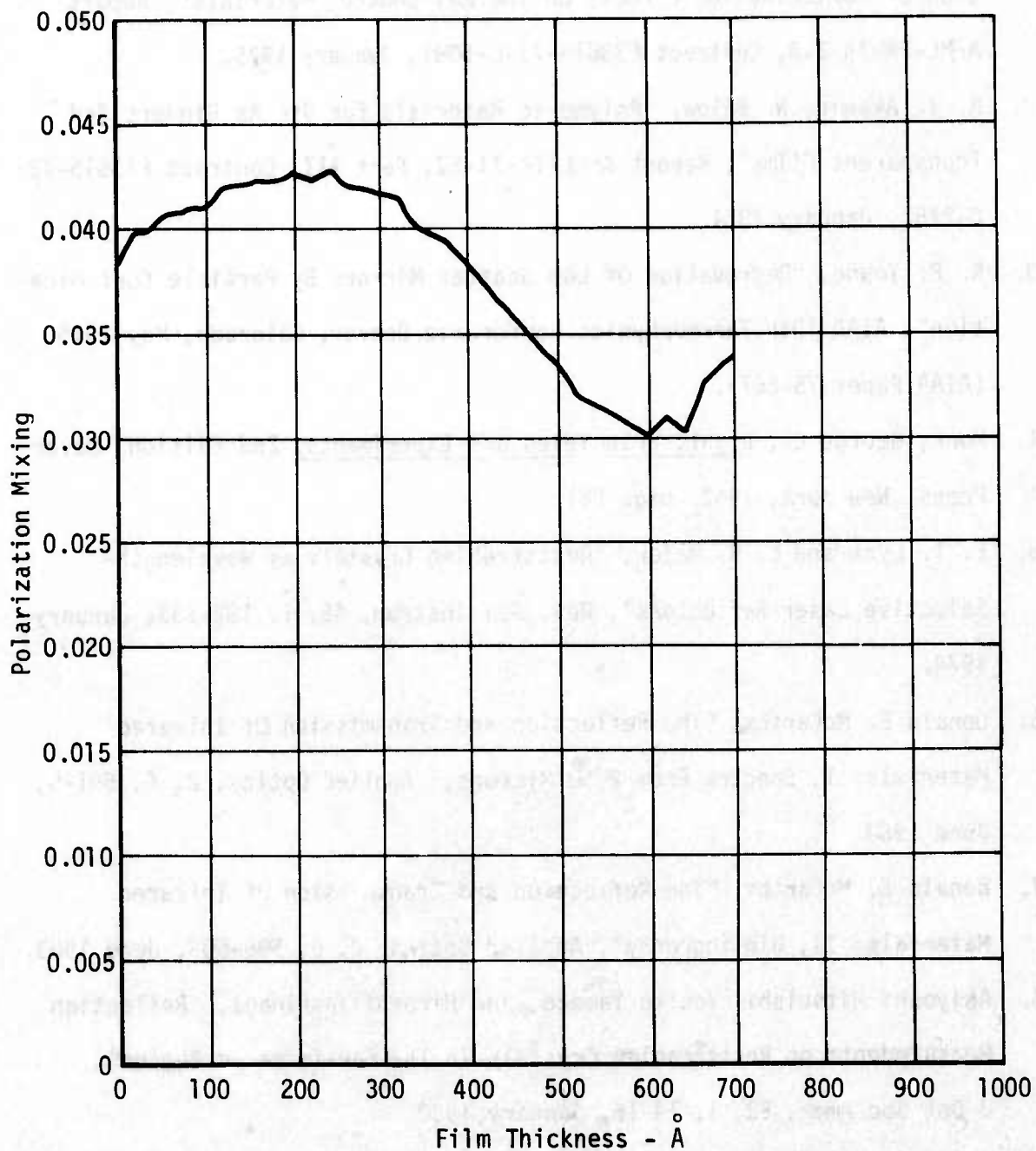


Figure 33 Polarization Mixing as a Function of Contaminant Thickness. Five-Layer Dielectric Stack on a Gold Mirror. Contaminant from RTV-106

VIII. REFERENCES

1. T. A. Hughes, T. H. Allen, R. M. F. Linford, T. E. Bonham, "Investigation Of Contamination Effects On Thermal Control Materials", Report AFML-TR-74-218, Contract F33615-73-C-5091, January 1975.
2. R. I. Akawie, N. Bilow, "Polymeric Materials For Use As Binders And Transparent Films", Report AFML-TR-71-62, Part III, Contract F33615-72-C-2157, January 1974.
3. R. P. Young, "Degradation Of Low Scatter Mirrors By Particle Contamination", AIAA 10th Thermophysics Conference, Denver, Colorado, May 1975 (AIAA Paper 75-667).
4. Monk, George C., Light, Principles and Experiments, 2nd Edition, Dover Press, New York, 1963, page 281.
5. E. T. Lynk and L. B. Major, "Reststrahlen Crystals as Wavelength-Selective Laser Reflectors", Rev. Sci Instrum, 45, 1, 132-133, January 1974.
6. Donald E. McCarthy, "The Reflection and Transmission Of Infrared Materials: I, Spectra From 2-50 Microns," Applied Optics, 2, 6, 591-5, June 1963.
7. Donald E. McCarthy, "The Reflection and Transmission Of Infrared Materials: II, Bibliography", Applied Optics 2, 6, 596-603, June 1963.
8. Akiyoshi Mitsuishi, Yohiko Yamada, and Hiroshi Yoshinaga, "Reflection Measurements on Reststrahlen Crystals In The Far-Infrared Region", J Opt Soc Amer, 52, 1, 14-16, January 1962.
9. Akiyoshi Mitsuishi, Yohiko Yamada, and Hiroshi Yoshinaga, "Transmission Filters In The Far-Infrared Region", J Opt Soc Amer, 52, 1, 17-19, January 1962.

VIII. REFERENCES (Continued)

10. E. D. Washburn, Editor, International Critical Tables, McGraw-Hill New York, Vol. V, Page 261.
11. American Institute of Physics Handbook, 3rd Edition, McGraw-Hill, New York, Pages 6-163, -169 and 6-280, -282.
12. Strong, Concepts In Classical Optics, W. H. Freeman, San Francisco, 1958, Pages 591-593.
13. Strong, Procedures In Experimental Physics, Prentice-Hall, 1938, Pages 367-369.
14. A. J. Moses, Handbook of Electronic Materials, Vol. I, Optical Material Properties; IFI/Plenum, New York 1971.
15. A. Goldsmith, H. J. Hirschhorn, T. E. Waterman, "Thermophysical Properties Of Solid Materials", Vol. III - Ceramics; WADC TR 58-476, Sect. VIII-D-1-a.
16. Proceedings Of The 1973 DOD Laser Effects/Hardening Conference (U), Vol. III, June 1974, pps. 74-81. (Document is SECRET, pages cited are unclassified).
17. W. G. Spitzer, D. A. Kleinman, "Infrared Lattice Bands Of Quartz", Physical Review, 121, 5, 1324-1335, March 1961.
18. H. Y. B. Mar, R. E. Peterson, Research On Selectivity Transmitting Infrared Materials (U), AFML TR-74-62, Contract F33615-73-C-5144, (SECRET).

AD

BO14104

AUTHORITY:

AFWAL

1tr, 19 NOV 82

